Adaptive reorganization of the cytoplasm upon stress in budding yeast

Guendalina Marini[1], Elisabeth Nüske[1], Weihua Leng[1], Simon Alberti[1], Gaia Pigino[1*]

1 Max Planck Institute of Molecular Cell Biology and Genetics, Dresden, Germany

* Correspondence to: pigino@mpi-cbg.de

Abstract

Yeast cells exposed to stress conditions such as starvation can enter a protective dormant state in which cell division, growth and metabolism are reduced or downregulated. They can remain in that state until nutrients become available again. How cells enter this dormant state and why it is protective is largely unknown. Here we use correlative light and electron microscopy and electron tomography to investigate the ultrastructural changes in the cytoplasm of starved yeast cells. We report that starved yeast cells undergo an extensive cytoplasmic reorganization that involves the formation of both membrane-bound and membraneless organelles. By determining the density of ribosomal particles, we show that the cytoplasm of starved yeast also experiences significant compaction. We further demonstrate that the key enzyme eukaryotic translation initiation factor 2B (eIF2B) polymerizes into large bundles of filaments through a reversible process. We propose that these changes allow yeast cells to store and inhibit proteins, and thus endure unfavorable environmental conditions.

Introduction

To survive in a constantly changing world, cells require mechanisms to cope with environmental changes. For instance, the baker's yeast *Saccharomyces cerevisiae* responds to sudden changes in nutrient abundance by adjusting its metabolism and growth rate. Under starvation conditions, yeast proliferation is efficiently shut down in favor of an energy-saving dormant state that allows the cells to remain viable with slow metabolic activity [Werner-Washburne et al., 1993; Choder, 1993; Ireland et al, 1994; Gray et al., 2004]. However, the mechanisms by which cells can enter and exit this dormant state remain unclear.

Recent findings suggest that yeast cytoplasm undergoes changes not only during different stages of the cell cycle but also in response to stress conditions, such as heat shock, osmotic stress, and nutrient starvation [Meaden et al, 1999; Winderickx et al., 2003; Petrovska et al., 2014; Mourão et al., 2014; Munna et al., 2015; Joyner et al., 2016; Munder et al., 2016]. The transition from a growing to a dormant state is coupled to a reduction in cell size and a decreased mobility of molecules in the cytoplasm, as well as decreased protein synthesis and metabolism [Ashe et al., 2000; Munder et al., 2016]. Interestingly, live-cell imaging shows that several metabolic enzymes condense in the cytoplasm of dormant cells [Narayanaswamy et al., 2009; Noree et al., 2010; Liu, 2010; Petrovska et al., 2014; Riback et al., 2017; Prouteau et al., 2017]. Electron microscopy analysis of two of these metabolic enzymes, cytidine triphosphate synthetase (CTPS) and glutamine synthetase (Gln1) [Barry et al., 2011; Petrovska et al., 2014], revealed that they assemble into large bundles of filaments. This polymerization process is coupled to the silencing of the CTPS and Gln1 enzymatic activities, suggesting that widespread formation of inactive assemblies might underlie the downregulation of metabolism in dormant cells. However, how the cytoplasm is reorganized during dormancy and stress conditions is still unclear and comprehensive structural investigations of dormancy-induced cytoplasmic changes are missing.

In this study, we used electron tomography (ET) to investigate the reorganization of the cytoplasm of energy-depleted yeast cells and correlative light and electron microscopy (CLEM) to study the behavior of the essential metabolic enzyme eIF2B (eukaryotic translation Initiation Factor 2B), a key guanine nucleotide exchange factor fundamental for protein synthesis. We show that energy-depleted cells undergo a dramatic reorganization the cytoplasm that involves

the formation of both membrane-bound and membraneless organelles, along with a two-fold increase in macromolecular crowding. Our results show that eIF2B self-assembles from an active soluble decameric form into ordered bundles of filaments. Based on these data, and those of the accompanying manuscript by Nüske et al., we propose that eIF2B compartmentalization is a mechanism to store and protect the enzyme from degradation, and possibly to regulate eIF2B enzymatic activity. These results are consistent with a model in which cytoplasmic reorganization and the self-assembly of essential enzymes are important survival strategies that enable cells to cope with extreme environmental conditions and stress.

Results

Dormancy is accompanied by characteristic cytoplasmic reorganization

To investigate whether the cytoplasm of stressed cells undergoes structural rearrangements, we imaged control and energy-depleted yeast cells by electron tomography. Cells were cryo-fixed by high-pressure freezing to ensure the rapid immobilization of all macromolecular components in the cytoplasm, thus avoiding potential structural alterations that might occur during the slower process of standard chemical fixation [Frank, 2006]. Energy-depleted dormant cells were characterized by numerous ultrastructural changes (Fig.1, VideoS1 for a control cell, VideoS2-S3 for energy-depleted cells). For instance, we observed an increased number of small lipid droplets, recognizable by their amorphous non-electron-dense content, which appeared fragmented and of irregular shape compared to the control (Fig.1B,C). The average diameter of lipid droplets for control cells was ~250 nm, whereas the average diameter was reduced to ~120 nm in energy-depleted cells. The fragmentation of lipid droplets is indicative of changes in the regulation of lipid metabolism upon nutrient depletion.

Tonoplast invaginations and accumulation of membranous elongated structures also appeared in energy-depleted cells (Fig. 1B,D). These structures could extend up to 1 μm in length, with diameters ranging from 20 to 100 nm. The presence of tonoplast invaginations in energy-depleted cells supports the previously observed reduction in cell volume, which is attributed to a sudden water loss [Munder et al., 2016]. In some stressed cells we also observed spherical double-layered membrane vesicles containing mostly ribosomes. These resembled early autophagosomes (Fig.S1), often in an open pre-fusion conformation, but they were smaller than

would be expected for a mature autophagosome. Therefore, these structures could indicate early steps in the autophagy process.

Interestingly, energy-depleted cells contained cytoplasmic areas that lacked ribosomes and other larger macromolecular complexes, but these regions were not observed in controls. These areas were not delimited by membranes and all showed a clear separation from the rest of the cytoplasm irrespective of their morphology, which ranged from amorphous aggregate-like bodies to highly ordered filamentous structures (Fig.1B,C,E, Fig. 3C,E,H). These stress-induced exclusion areas could represent specialized membraneless compartments that contain specific macromolecular components, such as proteins or RNAs. These compartments did not show any specific distribution in the cytoplasm, nor specific interaction with organelles or cellular components.

Ribosome density is a direct read-out for cytoplasmic crowding in starved cells

A previous study of energy-depleted yeast reported an increased mechanical stability of the cytoplasm and a 7-15% reduction in cell volume [Munder et al., 2016; Joyner et al., 2016]. Based on these observations, it was proposed that macromolecular crowding might be increased in the cytoplasm of starved cells. However, a direct quantification of macromolecular crowding in cells is difficult to achieve, because starved cells also undergo significant changes in the size of internal organelles such as the vacuole [Joyner et al., 2016]. Therefore, a direct method for quantifying cytoplasmic density is needed to accurately determine the increase in crowding that starved cells experience.

Since ribosomes take up a significant fraction of the cellular interior [Duncan and Hershey, 1983; Warner 1999], quantifying the ribosome density could be used as a proxy for changes in cytoplasmic crowding. The identification of ribosomes in TEM images is relatively straightforward because ribosomes contain large amounts of negatively charged rRNAs, which increases the staining efficiency of the contrast agents used for TEM sample preparation. As a consequence, ribosomes are extremely electron dense and clearly distinguishable in TEM images (Fig.1B-E). However, in order to use ribosome density to quantify macromolecular crowding, we first had to verify that the ribosome number does not change significantly between

growing and dormant (energy-depleted) cells. This was addressed by immunoblot analysis, which showed no significant change in the amount of ribosomal proteins (Fig.2G). Moreover, previous work has shown that polysomes do not disassemble into 40S and 60S subunits upon starvation but remain intact as 80C monosomes [Kuhn et al [2001].

To quantify ribosome density, we developed a FIJI [Schindelin et al., 2012] macro to automatically detect and count ribosomes in tomographic slices. The images were processed by filtering (Fig.2A1 and B1), binarization (Fig.2A2 and B2), segmentation (Fig.2A3 and B3) and particle detection (Fig.2A4 and B4). The accuracy of the automated quantification workflow was tested by comparison to ground truth data generated by manual counting of the ribosomes in single tomographic slices (Fig. S2). Ribosomes were also manually counted in tomograms to obtain a volumetric quantification of the ribosome densities. The quantifications showed an almost two-fold increase in ribosome density in energy-depleted cells (Fig.2E,F; Fig.S2), which experience a dramatic increase in macromolecular crowding upon energy starvation. From these data, we estimate a reduction of the cytoplasmic volume of about 42%, which is far more pronounced than previous estimates based on cell volume measurements [Munder et al., 2016; Joyner et al., 2016]. This indicates that cell volume changes are not a good indicator of macromolecular crowding in yeast cells, and that alternative strategies, such as the one proposed here, are necessary to accurately determine crowding conditions in cells.

eIF2B forms filament bundles in energy-depleted cells

Macromolecular crowding has been proposed to promote the formation of enzyme assemblies in the cytoplasm of stressed cells [Petrovska et al., 2014; Joyner et al. 2016; Munder et al., 2016]. Indeed, previous fluorescence microscopy studies demonstrated that many enzymes form condensates and assemblies in starved cells. For example, Gln1 and CTPS were identified as enzymes that polymerize into protein-specific, ordered filaments upon energy depletion [Petrovska et al., 2014; Barry et al., 2014]. However, one caveat of these studies is that they relied on tagging with fluorescent proteins, which could increase a protein's ability to assemble. Using label-free TEM, we observed that energy-depleted cells contain a large number of amorphous condensates, filaments and bundles of proteins (Fig.1B-E and Fig.3C,E,H). This supports the idea that assemblies are abundant in stressed cells and suggests that many of the previously described structures are not due to tagging artifact and

thus may serve a physiological function.

One type of assembly that was very prominent in energy-depleted cells were large bundles of filaments. To determine the identity of this assembly, we performed correlative light and electron microscopy (CLEM). We focused on the eukaryotic translation initiation factor 2B (eIF2B), because it has been shown previously to form large condensates upon energy depletion by fluorescence microscopy [Hinnebusch and Lorsch, 2012; Noree et al. 2010]. First, we confirmed that GFP-tagged eIF2B forms condensates in yeast cells using our energy depletion conditions (Fig. S3 – Video S4). In agreement with previous work [Noree et al., 2010], eIF2B showed a diffuse cytoplasmic signal in growing cells (Fig. S3A), but after energy depletion, it rapidly concentrated into foci and elongated structures (~15 minutes) (Fig.S3B). At the same time, cell growth and division were arrested (Fig. S3B). We also observed that upon energy replenishment the fluorescence signal promptly became diffuse again (~15 minutes), and soon afterwards cells resumed growth (~30 minutes) (Fig.S3C – Video S4).

Next, we prepared cells for CLEM and, by selecting cell sections containing the fluorescence signal, we observed that eIF2B localized in membraneless compartments in energy-depleted cells (Fig.3, Fig.S4). We next obtained electron tomograms from cells expressing endogenous eIF2B-GFP and cells overexpressing eIF2B-GFP in. These tomograms revealed that eIF2B organizes into a specific type of large assembly, where numerous long filaments are packed in an aligned bundle. eIF2B filaments and bundles have a defined morphology, which distinguish them from other condensates and assemblies in stressed cells (Fig.3C,F-H). Several eIF2B bundles could be observed in individual cells, with overexpressing cells showing larger bundles.

Individual filaments appeared to have a characteristic zigzag shape with an approximate diameter of 15 nm and a longitudinal periodicity of about 14.5 nm. To investigate the 3D organization of the filaments in the bundle, we quantified the length and the distance between filaments (Fig. 4 – Video S5). The length of the filaments varied from ~45 nm to ~850 nm. The shorter filaments, which can be as short as three or four copies of the decameric eIf2B holoenzyme, were usually observed at the periphery of the bundle. The longest filaments were observed in cells that overexpressed eIF2B. The filaments were mostly aligned in regular rows, with a between-row spacing of ~13 nm and within-row spacing of ~26 nm (Fig. 4 C,D,E and Fig. 6A). The diameter, periodicity and spacing of eIF2B filaments in the bundle differed from

the ones of previously characterized enzymatic polymers, including those composed of other metabolic enzymes such as Gln1 and CTPs [Petrovska et al., 2014; Barry et al., 2014]. In stressed cells, we also observed filaments with a similar morphology and subunit repeat (~6 nm) to the ones described for Gln1 [Petrovska et al., 2014], which had a smoother appearance and a smaller diameter and between-filament spacing (~9 nm) than eIF2B filaments (Fig. 3 F,H).

It has been reported that fluorescent proteins have a natural tendency to oligomerize and thus form aggregates or other higher-order structures [Zacharias et al., 2002; Snapp et al., 2003]. This poses a problem for applications where fluorescent proteins are used to visualize the cellular localization, dynamics, behavior, and oligomeric state of a protein. Therefore, we used two distinct approaches to test whether eIF2B bundle formation might be caused or enhanced by the GFP tag: i) immunofluorescence labeling of eIF2B tagged with the short HA polypeptide chain, and ii) electron tomography of the native untagged eIF2B bundles in energy-depleted wild type cells. Immunofluorescence experiments of two distinct HA-tagged subunits of the eIF2B complex, the regulatory subunit Gcn3 (α) and the catalytic subunit Gcd1 (γ), revealed eIF2B foci and assemblies in energy-depleted cells (Fig.S5). TEM analysis of energy-depleted, wild type cells, with untagged endogenous or overexpressed eIF2B, revealed bundles of filaments with the characteristic morphological features of eIF2B (Fig.5) as observed also in the CLEM experiments. Notably, eIF2B bundles were larger in overexpressing cells (Fig. 5 A) than in wild type cells (Fig. 5 B-F). These results demonstrate that the GFP tag is not involved in the formation of eIF2B filaments and bundles, indicating the filament formation and bundling is an intrinsic property of the eIF2B.

In all analyzed tomograms of stressed cells, molecular complexes such as ribosomes or proteasomes were excluded from the space occupied by the eIF2B bundles. Additionally, eIF2B filaments and bundles were never associated with early autophagosomes, which often engulfed other cytoplasmic components in energy-depleted cells. These data suggest that compartmentalization of eIF2B in the bundles is a mechanism to protect the enzyme from degradation.

eIF2B filaments comprise repeating decamers

Because of their apparent repeating structure, eIF2B filaments are likely to represent polymers of a single protein complex. We therefore used a subtomogram averaging approach to obtain a rough 3D model of the repeating unit. The 3D model showed a zigzag pattern with a 14.5 nm repeat (Fig.6C) that reproduces the pattern visible in the raw tomograms (Fig.3; Fig.4; Fig.6D). The filament section had a long diameter of 16 nm and a short diameter of 13.5 nm (Fig.6C). Contact points between neighboring filaments were visible in the 3D model (Fig. 6 A, B) as they protruded from both sides of the zigzag shape. Such contact points were often visible also in the raw tomograms (Fig.6D; video S3). We cannot exclude the possibility that such thin connections could have been generated by the crosslinking and staining processes during sample preparation. However, the regularity of the inter-filament packing, where a central filament is surrounded by six or seven equidistant neighboring ones (Fig.4; Fig.6A), suggests that the observed lateral connections contribute to keeping the distance and pattern in the untreated native bundle.

We used a sample preparation protocol that includes cryo-fixation, freeze substitution and resin embedding. This approach does not allow the generation of high-resolution 3D models. As an alternative approach, we compared our model to a heavily filtered version of the recently published crystal-structure of the eIF2B decamer from *Schizosaccharomyces pombe* and *Homo sapiens* [Kashiwagi et al., 2016; Tsai et al., 2018; Zyryanova et al., 2018]. We detected reasonable similarities in size and shape (Fig.7). Figure 7 shows a proposed stacking of eIF2B decamers in the 3D model of the filament obtained by subtomogram averaging, which indicates that the majority of the filament and bundle densities are occupied by eIF2B. Although we cannot completely rule out the presence of other smaller proteins in the structure of the filaments, our data indicates that those could be generated by polymerization of eIF2B decamers alone. The stacking model we put forward suggests an intra-particle dimerization interface on Gcn3 (α) subunits and another inter-particle dimerization interface that involves the Gcd6 (ε) and Gcd1 (γ) subunits. We propose that these two interfaces promote filament polymerization.

Discussion

In this paper, we demonstrate that entry of yeast cells into a dormant, energy-depleted state is associated with a dramatic molecular and structural reorganization of the cytoplasm. We reveal that this process involves a pronounced increase in macromolecular crowding, a massive rearrangement of membranous structures and lipid storage bodies, and the *de novo* formation of a variety of assemblies and membraneless compartments. Using CLEM, we show that one of these assemblies is generated by the polymerization of the translation initiation factor eIF2B. Our findings and those of the accompanying paper from Nüske et al. provide evidence that the formation of higher-order structures is a key mechanism to store and protect essential enzymes and regulate their activity. We propose that cytoplasmic reorganization and enzyme self-assembly is an adaptive survival strategy that enable cells to cope with extreme environmental conditions and stress.

Fragmentation and increase of lipid droplets upon energy depletion

We observed many ultrastructural changes in energy-depleted yeast cells. One prominent feature of energy-depleted cells was changes in lipid droplet morphology. Normally, when yeast cells reach stationary phase, they undergo a shift from a lipolytic to a lipogenic metabolism [Madeira et al., 2015]. This is thought to induce the accumulation of lipid droplets in yeast cells [Madeira et al., 2015]. However, in our experiments, we exposed yeast cells to severe energy depletion conditions, which resulted in a sudden lack of ATP. Under these conditions, the metabolism switches directly to beta-oxidation of fatty acids [Gray et al., 2004; Kurat et al., 2006]. In this case, energy is derived from the lipolysis of lipid deposits, as is also reflected in the presence of smaller and fragmented lipid droplets in our tomograms (Fig.1C). As has been proposed previously [Ariotti et al., 2012; Hashimoto et al., 2012; Thiam and Beller, 2017], the fragmentation of lipid droplets may contribute to increasing the total surface area that is accessible to lipases, thus enhancing lipolytic activity and increasing cellular ATP levels.

Autophagy is neither the first nor the fastest response to energy depletion in yeast cells

In our tomographic reconstructions of energy-depleted cells, we observed several elongated intracellular membranous structures. Sporadically, we also identified double membrane vesicles containing packed ribosomes (Figure 2 - figure supplement 5). Dynamic reorganization of intracellular membranes occurs during autophagy, a bulk protein degradation mechanism that is stimulated by starvation and contributes to cell survival by recycling constituents and maintaining energy levels [Takeshige et al., 1992]. In yeast, autophagy is associated with the formation of a large autophagosome (~ 1 µm), a double or multi-layered membrane structure that sequesters portions of cytoplasm and degrades them by fusion with the vacuolar membrane [Noda and Ohsumi, 1998]. Surprisingly, in our tomograms, the double membrane vesicles that contained cytoplasmic components were smaller than expected for a mature autophagosome. In fact, the structures that we observed were often in an open pre-fusion conformation, presumably representing early steps in the autophagy process (Fig. S1). This may be due to the fact that the cells did not experience a gradual reduction in energy as during entry into stationary phase, but rather a sudden and acute depletion of energy. Together, this suggests that starvation-induced autophagy is not a major strategy to adapt to sudden starvation conditions.

Plasma membrane invaginations increase upon energy depletion

We observed plasma membrane invaginations in energy-depleted cells (Fig.1B,D). These invaginations are morphologically similar to those of yeast cells exposed to severe dehydration [Dupont et al., 2010]. Yeast cells respond to changes in osmotic pressures with a loss of water and rapid shrinkage of the cell volume [Morris et al., 1986; Blomberg and Adler, 1992; Gervais and Marechal, 1994; Martinez de Maranon et al., 1996; Slaninova et al, 2000; Simonin et al., 2007]. This suggests that the plasma membrane invaginations in energy-depleted cells could be a compensatory mechanism to cope with a sudden loss of water. Why energy-depleted cells lose water is unclear. Most likely, this is the result of a misregulation of ion distributions across membranes arising from a lack of energy normally used for ion transporters and pumps.

Yeast cells that have experienced cell volume reduction have to expand their membrane surface again when the conditions improve. A rapid expansion of the plasma membrane

requires ‘membrane reservoirs' that buffer membrane tension and provide membrane surface area. Eisosomes, long invaginations in the plasma membrane of yeast, have been proposed to act as membrane reservoirs in an analogous manner to caveolae in animal cells [Kabeche et al. 2015]. Thus, it is possible that the invaginations that we observe in our tomograms are eisosomes. The accentuated depth of these invaginations suggests a rapid shrinkage of the membrane surface upon exposure of the cells to energy depletion. Upon energy replenishment, these eisosomal invaginations could provide the reservoir for prompt expansion of the plasma membrane and reestablishment of a normal cell volume.

Ribosome density is a measure of increased macromolecular crowding

We used ribosome quantification to determine the density of the cytosol and thus the extent of macromolecular crowding in stressed cells. While the total ribosome number remained unchanged, we observed an almost two-fold increase in ribosome density in energy-depleted cells. This shows a marked increase in crowding of the cytoplasm in yeast cells that are exposed to energy starvation conditions. This increase in cytoplasmic density most likely is the result of a loss water from the cytosol, and it is associated with an overall reduction in cell volume and a marked enlargement of the vacuole. Enlarged vacuoles have previously been observed in starved cells [Noda and Ohsumi, 1998; Joyner et al., 2016] as well as in cells exposed to other stresses [Desfougeres et al., 2016]. The molecular mechanisms of how cells regulate water release and uptake under stress conditions remain poorly understood. Regardless, the method proposed here promises to be a very reliable tool to determine the crowding conditions inside cells in response to environmental perturbations.

Macromolecular crowding and cytoplasm compartmentalization

Changes in molecular crowding can have profound effects on cytoplasm organization and on cell physiology [Rivas et al., 2001; Zhou et al., 2008]. Crowding can dramatically decrease molecular motion, resulting in steric hindrance of binding sites and consequent reduced rate of chemical reactions [Trappe et al., 2001; Miermont et al., 2013; Munder et al., 2016]. Crowding has also been shown to promote the formation of higher-order assemblies. In agreement with

this, we find that the cytoplasm of energy-depleted cells is populated by many membraneless higher-order structures with both amorphous and regular ultrastructure. A number of yeast enzymes are known to polymerize in the cytoplasm of starved cells [Narayanaswamy et al, 2009; Noree et al., 2010]. Among these, Gln1, CTPS [Petrovska et al., 2014; Barry et al., 2014] and, as we show in this study, eIF2B polymerize homotypically. In agreement with this, *in vitro* experiments have shown that, in simplified systems, formation of large protein assemblies such as enzyme filaments is promoted by addition of crowding agents [Petrovska et al., 2014; Woodruff et al., 2017].

However, an increase in crowding conditions is often not enough to induce the formation of higher-order structures. Energy-depleted yeast cells for example experience a sudden acidification of the cytosol [Petrovska et al., 2014; Munder et al., 2016]. This pH drop is thought to change surface charges of molecules, producing new repulsive and attractive molecular interactions in the cytoplasm. In agreement with this, changes in cytosolic pH are often sufficient to induce the formation of higher order assemblies, whereas changes in crowding conditions are not [Munder et al., 2016]. Therefore, cytosolic pH changes may initiate the formation of enzyme-specific assemblies in energy-depleted cells, whereas changes in crowding conditions have an enhancing effect that further stabilizes these assemblies when they are formed.

Assembly of filament bundles may protect eIF2B from degradation

eIF2B organizes into highly ordered bundles of long filaments in the cytoplasm of energy-depleted cells (Fig.3-6). The bundles are characterized by a very distinctive pattern of filament interspacing and polymer periodicity, which is different from the morphologies observed for other self-assembling metabolic enzymes. The polymeric nature of eIF2B filaments and the regular architecture of the bundles showed that these are the result of a coordinated self-assembly process of intact proteins, rather than the aggregation of misfolded proteins. A recent Cryo-EM study showed that aggregates of misfolded proteins, such as poly-Gly-Ala (poly-GA) in neurodegenerative diseases, are highly populated by 26S proteasomes, which are required for the degradation poly-GA [Guo et al., 2018]. However, in the case of eIF2B, ribosomes or proteasomes are excluded from eIF2B bundles. This indicates that the polymerization of eIF2B

proteins into bundles is a strategy to prevent protein degradation by the proteasome. Additionally, we never observed bundles of eIF2B engulfed into autophagosome vesicles, suggesting that filament formation could also be a protective mechanism against bulk protein degradation, such as autophagy. Therefore, we propose that the formation of bundles is a mechanism to reversibly store and protect eIF2B from degradation. Indeed, our work and that of Nüske et al [2018] show that upon replenishment of nutrients eIF2B enzymes are readily released in a soluble form and their nucleotide exchange activity is promptly reestablished.

eIF2B bundles form via polymerization at nucleation centers

How is eIF2B bundle formation achieved? One possibility is through a lateral zippering of single elongated filaments. Alternatively, bundling could be promoted through the polymerization of individual eIF2B enzymes around a nucleation center. In the first case, we would expect to find several isolated filaments in the proximity of a bundle, as they would approach the bundle after independent polymerization. However, in our tomograms we never observed such a distribution, and only very short filaments were present at the periphery of the bundle. Moreover, filament ends at the extremity of the bundle appeared to have a looser conformation, as would be expected if eIF2B enzymes would polymerize around a nucleation center. These ultrastructural features support the idea of a central nucleation mechanism. This mechanism implies the migration of individual enzyme complexes or small units of a few stacked enzyme complexes, instead of an entire, long filament, during the progressive crowding of the cytoplasm, thereby facilitating the assembly of eIF2B.

eIF2B forms filaments as a survival strategy against starvation

In a previous study, eIF2B condensates were observed in the cytoplasm of exponentially growing cells and were proposed to increase eIF2B nucleotide exchange rate [Campbell et al., 2005]. However, we only detected eIF2B filaments in cells exposed to starvation conditions, and never in growing cells. Campbell et al. [2005] used a dimerization-prone GFP tag that can indeed induce the formation of non-physiological eIF2B condensates in log-phase growing cells. Moreover, our investigation of filament formation in WT cells confirmed that filaments and

bundles can be found only in stressed cells. Our results suggest that eIF2B filament formation is a specific adaptation to conditions in which energy levels are low. This hypothesis is supported by the observation that translation is arrested in wild type energy-depleted cells [Nueske et al., 2018], and that their nucleotide exchange activity is promptly reestablished upon replenishment of nutrients through consequent release of eIF2B molecules in the dissolved form (Fig.S3, VideoS4). Moreover, yeast cells bearing mutant eIF2B, that are unable to form condensates, die faster than wild type cells in stationary phase [Nueske et al., 2018], suggesting that enzyme polymerization is indeed necessary for cell survival.

eIF2B filaments may form through interaction between the catalytic subunits

How does eIF2B assemble into filaments? To get insight into this question, we compared the crystal structure [Kashiwagi et al., 2016] and the cryo-EM structure of eIF2B decamers [Tsai et al., 2018, Zyryanova et al., 2018] with the periodicity and size of the filament-repeating unit (Fig.7). Our analysis suggests that filaments are formed by polymerization of eIF2B decamers. Decamers have been proposed to form through interaction of the Gcn3 (α) subunits [Wortham et al., 2014], which are components of the regulatory subcomplex. Based on our data, we propose that polymerization of the decamers occurs mainly through the catalytic subunit Gcd6 (ε). Interestingly, we could not accommodate the density of the Gcd1(γ) subunit, as it is known in the crystal structure, in our 3D model of the filament. The Gcd1(γ) subunit is indeed the least resolved also in the cryo-EM structures of eIF2B [Tsai et al., 2018, Zyryanova et al., 2018], indicating this subunit is conformationally flexible. Although our 3D reconstruction of the filament unit is not resolved enough to generate a conclusive model, we speculate that eIF2B might undergo conformational changes at the level of Gcd1(γ) and Gcd6(ε) subunits in order to polymerize into a filament. Polymerization through the catalytic subcomplex could also explain the silencing of eIF2B function when the enzyme is sequestered in the filaments [Nüske et al., 2018]. Thus, polymerization through conformational changes or direct protein-protein interactions in the polymer may occlude the catalytic active sites. Alternatively, polymerization may inhibit interactions with accessory factors that regulate eIF2B activity. Future studies of eIF2B filaments at higher resolution by cryo-EM will be necessary to clarify the molecular

mechanism involved in the filament formation and the molecular mechanism of enzyme inhibition.

In summary, we have described the adaptive rearrangements that take place in the cytoplasm of energy depleted yeast cells. We propose that these changes allow cells to save energy, store and regulate proteins and endure unfavorable environmental conditions. It remains to be investigated whether this cytoplasmic reorganization is a general response in other species and to other kinds of stress.

Materials and methods

Yeast strains, media and energy depletion

Wild type *Saccharomyces cerevisiae* W303 cells and the two strains overexpressing untagged and sfEGFP-tagged eIF2B [Nüske et al., 2018] were grown in an orbital shaker (180 rpm) at 25˚C in YPD medium containing 1% (w/v) yeast extract, 2% peptone, and 2% glucose. Detailed information on the generation of the mutant strains are published in a related study [Nüske et al., 2018].

Stress treatments were carried out on cells grown to mid-log phase and cellular growth was monitored by optical density (OD) at 600 nm. To induce energy depletion (ATP depletion), cells at 0.5 OD_{600nm} were washed twice and then incubated in SD (synthetic dropout) complete medium containing 20 mM 2-deoxyglucose (2-DG; Carl Roth GmbH, Karlsruhe, Germany) and 10 M antimycin-A (Sigma-Aldrich, Steinheim, Germany) for at least 15 minutes. These two chemicals were used to block glycolysis and mitochondrial respiration, respectively. In general, this treatment reduces intracellular ATP levels by more than 95% [Serrano, 1977]. Yeast samples were then incubated in an orbital shaker at 30˚C for 1 hour. Log phase yeast cells expressing only endogenous untagged eIF2B were treated in both complete and energy-depleted medium in the same way as described above.

Fluorescence microscopy

Yeast cells were imaged in concanavalin A-coated 4-well Matek dishes. Fluorescence microscopy of live (time-lapse movies) and fixed cells were acquired using a Deltavision microscope system with softWoRx 4.1.2 software (Applied Precision), 100x 1.4 NA UPlanSApo oil immersion objective, and CoolSnap HQ2 camera (Photometrics) at 1024x1024 (or 512x512) pixels. Exposure time was 0.3 seconds and the interval between consecutive frames in the time lapse was 15 minutes.

We determined the exact time required for yeast cells to enter the dormant state upon energy depletion by analysis of the fluorescence microscopy time-lapse movies. This information was required to select dormant cells for imaging in TEM and compare their ultrastructure with that of growing cells.

Immunostaining

For immunostaining, cells expressing GCD1-γ-HA and Gcn3-α-HA were fixed via treatment with 3.7% paraformaldehyde (EMS, Hatfield, USA) for at least 30 minutes followed by 45 minutes incubation in spheroplasting buffer (100 mM phosphate buffer pH 7.5, 5 mM EDTA, 1.2 M Sorbitol (Sigma-Aldrich, Steinheim, Germany), Zymolyase (Zymo Research, USA) at 30˚C with mild agitation. Spheroplasts were permeabilized with 1% triton X-100 (Serva, Heidelberg, Germany), washed and incubated with mouse anti-HA primary antibody (1:2000; Covance, USA) and goat anti-mouse-HRP (1:5000; Sigma, Saint Louis, USA).

High pressure freezing and freeze substitution of yeast cells

Yeast cells, harvested by vacuum filtration as described in Bertin and Nogales [2016], were transferred to 100 µm deep membrane carriers and high pressure frozen with a Leica EM PACT2 or Leica EM ICE freezers (Leica Microsystems, Wentzler, Germany). All samples were processed by freeze substitution in a Leica AFS2 temperature-controlling machine (Leica Microsystems, Wentzler, Germany) and then embedded in resin using two distinct protocols for untagged and GFP-tagged yeast strains.

Untagged eIF2B yeast cells: High pressure frozen samples were freeze substituted using 1% osmium tetroxide, 0.1% uranyl acetate (wt/vol) and 5% H_2O (vol/vol) in glass distilled acetone. Freeze substitution was carried out at -90˚C for 36 hours before raising the temperature steadily to -30˚C in 4˚C per hour. The samples were kept at -30˚C for 5 hours before they were brought to 0˚C in steps of 4˚C per hour. Samples were washed with acetone and infiltrated with increasing concentrations (25, 50, 75 and 100%; 2 h each) of EPON resin (Electron Microscopy Sciences). 100% EPON solution was exchanged two times in 12-hour steps. Resin infiltrated samples were then UV polymerized at 60˚C for 48 hours. Samples were cut into 150 to 200 nm sections with an ultramicrotome (Ultracut UCT; Leica) and an Ultra 35˚ diamond knife (Diatome). The sections were mounted on Formvar-coated slot grids (Science Services).

sfEGFP-tagged eIF2B yeast cells: Vitrified yeast cells were freeze substituted with 0.1% (wt/vol) uranyl acetate and 4% (vol/vol) water in acetone at -90˚C as described in Kukulski et al. [2011].

The samples were then embedded in Lowicryl HM-20 (Polysciences Inc.) and cut into 70, 100 and 150 nm thick sections using an ultramicrotome (Ultracut UCT; Leica) with a Ultra 35˚ diamond knife (Diatome).

Correlative light and electron microscopy

For CLEM imaging, sections from sfEGFP-tagged eIF2B yeast cells, embedded in Lowicryl HM-20 (Polysciences Inc.) [Kukulski et al., 2011], were mounted on Formvar-coated finder grids (Science Services) and incubated with Quenched Blue FluoSphere fiducials (200 nm diameter) diluted 1:500 for 10 minutes in the dark. Grids were mounted on a glass slide with VectaShield (Vector Laboratories, Inc., Burlingame, USA) and imaged with a Zeiss Axioplan2 wide-field fluorescence CCD upright microscope to record the fluorescence signal in sections of the embedded yeast cells. Images were acquired with a 10x objective lens to generate a grid overview and a 100x objective lens (na. 1.4) to image the fluorescence in individual cells. Cells were imaged with a green GFP channel (488 nm) for the sfEGFP-tagged eIF2B and a UV channel (nm) for the Blue FluoSphere fiducials. The correlation (overlay) between the images obtained in fluorescence microscopy and EM micrographs or tomographic slices was performed with AMIRA® 3D Visualization & Analysis Software (FEI Company - http://www.vsg3d.com/amira/)(Zuse-Institut, Berlin, Germany).

Electron tomography

All sections from resin embedded samples were stained with 1% (wt/vol) uranyl acetate for 5 minutes and 70% lead citrate for 3 minutes. Colloidal gold particles (15 nm) were added to both surfaces of the sections to serve as fiducial markers for tilt series alignment. Tomographic series were acquired in dual-axis tilt scheme (±60˚ and 1˚ increments) with SerialEM [Mastronarde, 2005], using a FEI Tecnai F30 TEM (300 kV) equipped with Gatan US1000 CCD camera. Pixel size ranged between 7-12Å/px. Tomograms reconstruction was performed using the IMOD package [Mastronarde, 1997].

Subtomogram averaging

Subtomogram averaging was done with PEET software from the IMOD package [Heumann et al., 2011]. Subtomograms with a dimension of 54x54x54 voxels (40x40x40 nm) were

automatically picked along eIF2B filaments every 15 nm. A final average was calculated from a total of 500 particles. A loose mask was used to refine the central filament average. Semi-automatic segmentation of structures of interest in the tomograms was obtained with the software SuRVoS [Luengo et al., 2017]. The USCF Chimera package was used for 3D visualization, rendering, and animation of the reconstructed volumes [Pettersen et al., 2004].

Acknowledgments

We acknowledge JR. Warner and SV. Buhl, from the Albert Einstein College of Medicine (NY) for kindly providing us the L3 (TCM) monoclonal and the L30/S4 polyclonal ribosome antibodies. We thank T. Müller-Reichert for sharing the Amira protocol of automated filament tracing, and D. Richter for cloning HA-tagged eIF2B yeast strains. We gratefully acknowledge T. Furstenhaupt, K. Gibson and the EM Facility at the Max Planck Institute of Molecular Cell Biology and Genetics (MPI-CBG) for their support. We thank O Gonzalez for IT support and F. Jug for substantial advice and theoretical input. This work was supported by the Dresden International Graduate School for Biomedicine and Bioengineering (DIGS-BB), granted by the German Research Foundation (DFG) in the context of the Excellence Initiative. EN and SA were supported by a grant of the German Research Foundation (DFG, AL 1061/5–1) and SA had additional funding from Human Frontiers Program grant RGP0034/2017 and the Volkswagen “Life?” initiative.

Author contributions

GM: experimental design, data acquisition, data analysis and interpretation, manuscript writing. EN: experimental design, data acquisition, data interpretation. WL: support for data acquisition. SA: conception and design, manuscript writing. GP: conception and design, data analysis and interpretation, manuscript writing.

Figures and Supplementary material

See FiguresJCB.pdf

REFERENCES

. Adya, A.K., Canetta, E. and G.M. Walker. 2006. Atomic force microscopic study of the influence of physical stresses on *Saccharomyces cerevisiae* and *Schizosaccharomyces pombe*, FEMS Yeast Res. 6 120–128.

. Ariotti, N., Murphy, S., Hamilton, N., Wu, L., Green, K., Schieber, N.L., Li, P. and P.G. Parton. 2012. Postlipolytic insulin-dependent remodeling of micro lipid droplets in adipocytes. Mol Biol Cell May 15; 23(10):1826–1837 doi: 10.1091/mbc.E11-10-0847

. Ashe, M.P., De Long, S.K. and A.B. Sachs. 2000. Glucose depletion rapidly inhibits translation initiation in yeast. Mol. Biol. Cell *11*, 833-848.

. Barry, R.M., Bitbol, A.F., Lorestani, A., Charles, E.J., Habrian, C.H., Hansen, J.M., Li, H.J., Baldwin, E.P., Wingreen, N.S., Kollmanand, J.M. and Z. Gitai. 2014. Large-scale lament formation inhibits the activity of CTP synthetase. eLife 14, e03638.

. Bertin, A. and E. Nogales. 2016. Characterization of septin ultrastructure in budding yeast using electron tomography. Yeast Cytokinesis: Methods and Protocols. Springer New York - Sanchez-Diaz A. and Perez P.

. Blomberg, A. and L. Adler. 1992. Physiology of osmotolerance in fungi, Adv. Microb. Physiol. 33:145–212.

. Cameron, I., Kanal, K. and G. Fullerton. 2006. Role of protein conformation and aggregation in pumping water in and out of a cell. Cell Biology International 30:78–85. doi: 10.1016/j.cellbi.2005.09.010

. Cameron, I.L. and G.D. Fullerton. 2014. Lack of appreciation of the role of osmotically unresponsive water in cell volume regulation. Cell Biology International 38:610–614. doi: 10.1002/cbin.10238

. Campbell, S.G., Hoyle, N.P. and M.P. Ashe. 2005. Dynamic cycling of eIF2 through a large eIF2B-containing cytoplasmic body implications for translation control. J Cell Biol. 170(6): 925–934. doi:10.1083/jcb.200503162

. Choder, M. 1993. A growth rate-limiting process in the last growth phase of the yeast life cycle involves RPB4, a subunit of RNA polymerase. J Bacteriol. 175:6358–63.

. Desfougeres, Y., Neumann, H., and A. Mayer. 2016. Organelle size control – increasing vacuole content activates SNAREs to augment organelle volume through homotypic fusion. J. Cell Sci. 129, 2817-2828.

. Duncan, R. and J.W. Hershey. 1983. Identification and quantitation of levels of protein synthesis initiation factors in crude HeLa cell lysates by two-dimensional polyacrylamide gel electrophoresis. J Biol Chem. 10;258(11):7228-35.

. Dupont, S., Beney, L., Ritt, J.F., Lherminier, J. and P. Gervais. 2010. Lateral reorganization of plasma membrane is involved in the yeast resistance to severe dehydration. Biochim Biophys Acta. May;1798(5):975-85. doi: 10.1016/j.bbamem.2010.01.015. Epub 2010 Jan 28.

. Frank, J. .2006. Three-Dimensional Electron Microscopy of Macromolecular Assemblies: Visualization of Biological Molecules in their Native State. Oxford University Press, Inc.

. Fullerton, G.D., Kanal, K.M. and I.L. Cameron. 2006. Osmotically unresponsive water fraction on proteins: non-ideal osmotic pressure of bovine serum albumin as a function of pH and salt concentration. Cell Biology International 30:86–92. doi: 10.1016/j.cellbi.2005.11.001

. Gervais, P. and P.A. Marechal. 1994.Yeast resistance to high levels of osmotic pressure: influence of kinetics, J. Food Eng. 22:399–407.

. Gordiyenko, Y., Schmidt C., Jennings M.D., Matak-Vinkovic, D., Pavitt, G.D. and C.V. Robinson. 2014. eIF2B is a decameric guanine nucleotide exchange factor with a gamma2epsilon2 tetrameric core. Nat Commun 5:3902. doi: 10.1038/ncomms4902.

. Gray J.V., Petsko G.A., Johnston G.C., Ringe D., Singer R.A. and M. Werner-Washburne. 2004. “Sleeping Beauty: Quiescence in *Saccharomyces cerevisiae*.” In: Microbiol Mol Biol Rev 68(2):187–206.

. Gray, J.V., Petsko, G.A., Johnston, G.C., Ringe, D., Singer, R.A., and M. Werner-Washburne. 2004."Sleeping Beauty": Quiescence in *Saccharomyces cerevisiae*. Microbiol. Mol. Biol. Rev. 68(2):187–206.

. Guo, Q., Lehmer, C., Martínez-Sánchez, A., Rudack, T., Beck, F., Hartmann, H., Pérez-Berlanga, M, Frottin, F., Hipp, M.S., Hartl, F.U., Edbauer, D., Baumeister, W. and R. Fernández-Busnadiego. 2018. In Situ Structure of Neuronal C9orf72 Poly-GA Aggregates Reveals Proteasome Recruitment. Cell. 172(4):696-705. e12. doi: 10.1016/j.cell.2017.12.030.

. Hashimoto, T., Segawa, H., Okuno, M., Kano, H., Hamaguchi, H.-O., Haraguchi, T., Hiraoka, Y., Hasui, S., Yamaguchi, T., Hirose, F. and T. Osumi. 2012. Active involvement of micro-lipid droplets and lipid-droplet-associated proteins in hormone-stimulated lipolysis in adipocytes. J. Cell Sci. 125, 6127-6136.

. Heumann, J., Hoenger, A. and D. Mastronarde. 2011. Clustering and variance maps for cryo-electron tomography using wedge-masked differences. J Struct Biol. 175(3):288–299.

. Hinnebusch, A.G. and J.R. Lorsch. 2012. The mechanism of eukaryotic translation initiation: new insights and challenges. Cold Spring Harb Perspect Biol. 4(10). pii: a011544. doi: 10.1101/cshperspect.a011544.

. Ireland, L.S., Johnston, G.C., Drebot, M.A., Dhillon, N., DeMaggio, A.J., Hoekstra, M.F., and R.A. Singer. 1994. A member of a novel family of yeast ‘Zn-finger’ proteins mediates the transition from stationary phase to cell proliferation. EMBO J. 13:3812–21.

. Jorgensen, P., Rupěs, I., Sharom, J.R., Schneper, L., Broach, J.R. and M. Tyers. 2004. A dynamic transcriptional network communicates growth potential to ribosome synthesis and critical cell size. Genes Dev, 18(20):2491–505.

. Joyner, R.P., Tang, J.H., Helenius, J., Dultz, E., Brune, C., Holt, L.J., Huet, S., Müller, D.J. and K. Weis. 2016. A glucose-starvation response regulates the diffusion of macromolecules. eLife 5, e09376. doi: 10.7554/eLife.09376.

. Kabeche, R., Howard, L. and J.B. Moseley. 2015. Eisosomes provide membrane reservoirs for rapid expansion of the yeast plasma membrane. J Cell Sci. Nov 15;128(22):4057-62. doi: 10.1242/jcs.176867. Epub 2015 Sep 24.

. Kashiwagi, K., Takahashi, M., Nishimoto, M., Hiyama, T.B., Higo, T., Umehara, T., Sakamoto, K., Ito T. and S. Yokoyama. 2016. Crystal structure of eukaryotic translation initiation factor 2B. Nature, 531:4–52.

. Kuhn, K.M., Derisi, J.L., Brown, P.O. and P. Sarnow. 2001. Global and Specific Translational Regulation in the Genomic Response of *Saccharomyces cerevisiae* to a Rapid Transfer from a Fermentable to a Nonfermentable Carbon Source. Mol Cell Biol 21(3), 916–927.

. Kukulski, W., Schorb, M., Welsch, S., Picco, A., Kaksonen, M. and J.A. Briggs. 2011. Correlated fluorescence and 3D electron microscopy with high sensitivity and spatial precision. J Cell Biol 10;192(1):111–119.

. Kurat, C.F., Natter, K., Petschnigg, J., Wolinski, H., Scheuringer, K., Scholz, H., Zimmermann, R., Leber, R., Zechner, R., S.D. Kohlwein. 2006. Obese yeast: triglyceride lipolysis is functionally conserved from mammals to yeast. J Biol Chem, 281(1):491-500. Epub 2005 Nov 2.

. Lang, M.J., Martinez-marquez, J.Y., Prosser, D.C., Ganser, L.R., Buelto, D., Wendland, B. and M.C. Duncan. 2014. Glucose starvation inhibits autophagy via vacuolar hydrolysis and induces plasma membrane internalization by down-regulating recycling. J Biol Chem. 289:16736–16747. https://doi.org/10.1074/jbc.M113.525782

. Liu, J.L. 2010. Intracellular compartmentation of CTP synthase in Drosophila. J. Genet. Genom. 37(5):281-296

. Luengo, I., Darrow, M., Spink, M., Sun, Y., Dai, W., He, C., Chiu, W., Pridmore, T., Ashton, A., Duke, E., Basham M. and A. French. 2017. SuRVoS: Super-Region Volume Segmentation workbench. J Struct Biol. 198(1):43–53.

. Madeira, J.B., Masuda, C.A., Maya-Monteiro, C.M., Matos, G.S., Montero-Lomelí, M., B.L. Bozaquel-Morais. 2015. TORC1 inhibition induces lipid droplet replenishment in yeast. Mol Cell Biol, 35(4):737-46. doi: 10.1128/MCB.01314-14.

. Martinez de Maranon, I., Marechal, P.A. and P. Gervais. 1996. Passive response of *Saccharomyces cerevisiae* to osmotic shifts: cell volume variations depending on the physiological state, Biochem. Biophys. Res. Commun. 227:519–523.

. Mastronarde, D. 1997. Dual-axis tomography: an approach with alignment methods that preserve resolution. J Struct Biol. 120(10):343–352.

. Mastronarde, D. 2005. Automated electron microscope tomography using robust prediction of specimen movements. J Struct Biol. 152(1):36–51.

. Matile, P., Moor. H. and C.F. Robinow. 1969. Yeast cytology. Academic Press: London. In "The Yeasts", vol. 1, pp. 219–301: Rose A.H., Harrison J.S.

. Meaden, P.G., Arneborg, N., Guldfeldt, L.U., Siegumfeldt, H. and M. Jakobsen. 1999. Endocytosis and vacuolar morphology in *Saccharomyces cerevisiae* are altered in response to ethanol stress or heat shock. Yeast, 15:1211-1222.

. Miermont, A., Waharte, F., Hu, S., McClean, M.N., Bottani, S., Léon, S. and P. Hersen. 2013. Severe osmotic compression triggers a slowdown of intracellular signaling, which can be explained by molecular crowding. Proc Natl Acad Sci USA Apr 2;110(14), 5725–5730.

. Moretto, F., Sagot. I., Daignan-Fornier, B. and B. Pinson. 2013. A pharmaco-epistasis strategy reveals a new cell size controlling pathway in yeast. Mol Syst Biol, 9(707):1-12.

. Morris, G.J., Winters, L., Coulson, G.E. and K.J. Clarke. 1986. Effect of osmotic stress on the ultrastructure and viability of the yeast *Saccharomyces cerevisiae*. J. Gen. Microbiol. 132:2023–2034.

. Mourão, M.A., Hakim, J.B. and S. Schnell. 2014. Connecting the dots: the effects of macromolecular crowding on cell physiology. Biophys J, 107(12):2761–2766.

. Munder, M.C., Midtvedt, D., Franzmann, T., Nüske, E., Otto, O., Herbig, M., Ulbricht, E., Müller, P., Taubenberger, A., Maharana, S., Malinovska, L., Richter, D., Guck, J., Zaburdaev, V. and S. Alberti. 2016. A pH-driven transition of the cytoplasm from a fluid- to a solid-like state promotes entry into dormancy. eLife 5, e09347.

. Munna, M.S., Humayun, S., and R. Noor. 2015. Influence of heat shock and osmotic stresses on the growth and viability of *Saccharomyces cerevisiae*. BMC Research Notes. 2015;8:369. doi:10.1186/s13104-015-1355-x.

. Narayanaswamy, R., Levy, M., Tsechansky, M., Stovall, G.M., O'Connell, J.D., Mirrielees, J., Ellington, A.D. and E.M. Marcotte. 2009. Widespread reorganization of metabolic enzymes into reversible assemblies upon nutrient starvation. Proc NatlAcadSciUSA. 106(25):10147-52.

. Noda, T. and Y. Ohsumi. 1998. Tor, a phosphatidylinositol kinase homologue, controls autophagy in yeast. J. Biol. Chem. 273:3963–3966.

. Noree, C., Sato, B.K., Broyer, R.M. and J.E. Wilhelm. 2010. Identification of novel filament-forming proteins in *Saccharomyces cerevisiae* and *Drosophila melanogaster*. J Cell Biol, 190:541–51.

. Petrovska, I., Nüske, E., Kulasegaran, G., Gibson, K., Munder, M.C., Malinovska, L., Richter, D., Verbavatz, J.M. and S. Alberti. 2014. Filament formation by metabolic enzymes is a specific adaptation to the energy-depleted cellular state. eLife, 3:e02409.

. Pettersen, E., Goddard, T., Huang, C., Couch, G., Greenblatt, D., Meng, E. and T. Ferrin. 2004. UCSF Chimera – a visualization system for exploratory research and analysis. J Comput Chem. 25(13):1605–12.

. Prouteau, M., Desfosses, A., Sieben, C., Bourgoint, C., Mozaffari, L.N., Demurtas, D., Mitra, A.K., Guichard, P., Manley, S. and R. Loewith. 2017. TORC1 organized in inhibited domains (TOROIDs) regulate TORC1 activity. Nature, 12;550(7675):265-269. doi: 10.1038/nature24021.

. Riback, J.A., Katanski, C.D., Kear-Scott, J.L., Pilipenko, E.V., Rojek, A.E., Sosnick, T.R. and D.A. Drummond. 2017. Stress-triggered phase separation is an adaptive, evolutionarily tuned response. Cell, 168:1028–1040.

. Rivas, G., Fernández, J.A. and A.P. Minton. 2001. Direct observation of the enhancement of noncooperative protein self-assembly by macromolecular crowding: indefinite linear self-association of bacterial cell division protein FtsZ. Proc Natl Acad Sci USA 98, 3150–3155.

. Rudra, D. and J.R. Warner. 2004. What better measure than ribosome synthesis? Genes Dev. 18(20):2431–36.

. Rußmayer, H., Bucheics, M., Gruber, C., Valli, M., Grillitsch, K., Modarres, G., Guerrasio, R., Klavins, K., Neubauer, S., Drexler, H., Steiger, M., Troyer, C., Chalabi, A.A., Krebieh, G., Sonntag, D., Zellnig, G., Daum, G., Graf, A.B., Altmann, F., Koellensperger, G., Hann, S., Sauer, M., Mattanovich, D. and B. Gasser. 2015. Systems-level organization of yeast methylotrophic lifestyle. BMC Biology, 13:80 DOI 10.1186/s12915-015-0186-5

. Schindelin, J., Arganda-Carreras, I., Frise, E., Kaynig, V., Longair, M., Pietzsch, T., Preibisch, S., Rueden, C., Saalfeld, S., Schmid, B., Tinevez, J.Y., White, D.J., Hartenstein, V., Eliceiri K., Tomancak P. and A. Cardona. 2012. Fiji: an open-source platform for biological-image analysis. Nat Meth, 9(7):676–682.

. Serrano, R. 1977. Energy requirements for maltose transport in yeast. Eur J Biochem 80(1):97-102.

. Simonin H., Beney L. and P. Gervais. 2007. Sequence of occurring damages in yeast plasma membrane during dehydration and rehydration: Mechanisms of cell death, Biochim Biophys Acta. 1768:1600–1610

. Slaninova, I., Sestak, S., Svoboda, A. and V. Farkas. 2000. Cell wall and cytoskeleton reorganization as the response to hyperosmotic shock in *Saccharomyces cerevisiae*. Arch. Microbiol. 173:245–252.

. Snapp, E.L., Hegde, R.S., Francolini, M., Lombardo, F., Colombo, S., Pedrazzini, E., Borgese, N. and J. Lippincott-Schwartz. 2003. Formation of stacked ER cisternae by low affinity protein interactions. J Cell Biol, 163(2):257–269.

. Takeshige, K., Baba, M., Tsuboi, S., Noda, T. and Y. Ohsumi. 1992. Autophagy in yeast demonstrated with proteinase-deficient mutants and conditions for its induction. J Cell Biol, 119(2):301–311.

. Thiam, A.R. and M. Beller. 2017. The why, when and how of lipid droplet diversity. J Cell Sci. 130(2):315-324. doi: 10.1242/jcs.192021. Epub 2017 Jan 3.

. Thiery, J.P., Macaya, G. and Bernardi, G. 1976. An analysis of eukaryotic genomes by density gradient centrifugation J Mol Biol 108(1):219-235

. Thirumalai, D., Reddy, G. and J.E. Straub. 2012. Role of water in protein aggregation and amyloid polymorphism. Accounts of Chemical Research 45:83–92. doi: 10.1021/ar2000869

. Trappe, V., Prasad, V., Cipelletti, L., Segre, P.N., and D.A. Weitz. 2001. Jamming phase diagram for a ractive particles. Nature 411, 772–775.

. Tsai, J.C., Miller-Vedam, L.E., Anand, A.A., Jaishankar, P., Nguyen, H.C., Renslo, A.R., Frost, A. and P. Walter. 2018. Structure of the nucleotide exchange factor eIF2B reveals mechanism of memory-enhancing molecule. Science, 359(6383)i: eaaq0939.

. Tsukada, M. and Y. Ohsumi. 1993. Isolation and characterization of autophagy- defective mutants of *Saccharomyces cerevisiae*. FEBS Lett. 333: 169–174.

. Warner, J.R. 1999. The economics of ribosome biosynthesis in yeast. Trends Biochem Sci. 24(11):437-40.

. Werner-Washburne, M., Braun, E., Johnston, G.C., and R.A. Singer. 1993. Stationary phase in the yeast *Saccharomyces cerevisiae*. Microbiol Rev. 57(2):383–401.

. Winderickx, J., Holsbeeks, I., Lagatie, O., Giots, F., Thevelein, J. and H. de Winde. 2003. Yeast Stress Responses - From feast to famine; adaptation to nutrient availability in yeast. Topics in Current Genetics, Vol. 1. Springer-Verlag Berlin Heidelberg: S. Hohmann/P.W.H. Mager (Eds.)

. Woodruff, J.B., Ferreira Gomes, B., Widlund, P.O., Mahamid, J., Honigmann, A. and A.A. Hyman. 2017. The Centrosome Is a Selective Condensate that Nucleates Microtubules by Concentrating Tubulin. Cell. 169(6):1066-1077.e10. doi: 10.1016/j.cell.2017.05.028.

. Wortham, N.C., Martinez, M., Gordiyenko, Y., Robinson, C.V. and C.G. Proud. 2014. Analysis of the subunit organization of the eIF2B complex reveals new insights into its structure and regulation. FASEB J. 28(5):2225-2237.

. Zacharias, D.A., Violin, J.D., Newton, A.C. and R.Y. Tsien. 2002. Partitioning of lipid-modified monomeric GFPs into membrane microdomains of live cells. Science, 296(5569):913–916.

. Zhou, H.X., Rivas, G. and A.P. Minton. 2008. Macromolecular crowding and confinement: biochemical, biophysical, and potential physiological consequences. AnnuRev Biophys 37, 375–397.

. Zyryanova, A.F., Weis, F., Faille, A., Alard, A.A., Crespillo-Casado, A., Sekine, Y., Harding, H.P., Allen, F., Parts, L., Fromont, C., Fischer, P.M., Warren, A.J. and D. Ron. 2018. Binding of ISRIB reveals a regulatory site in the nucleotide exchange factor eIF2B. *Science* 359(6383):1533-1536. DOI: 10.1126/science.aar5129

Fig. 1

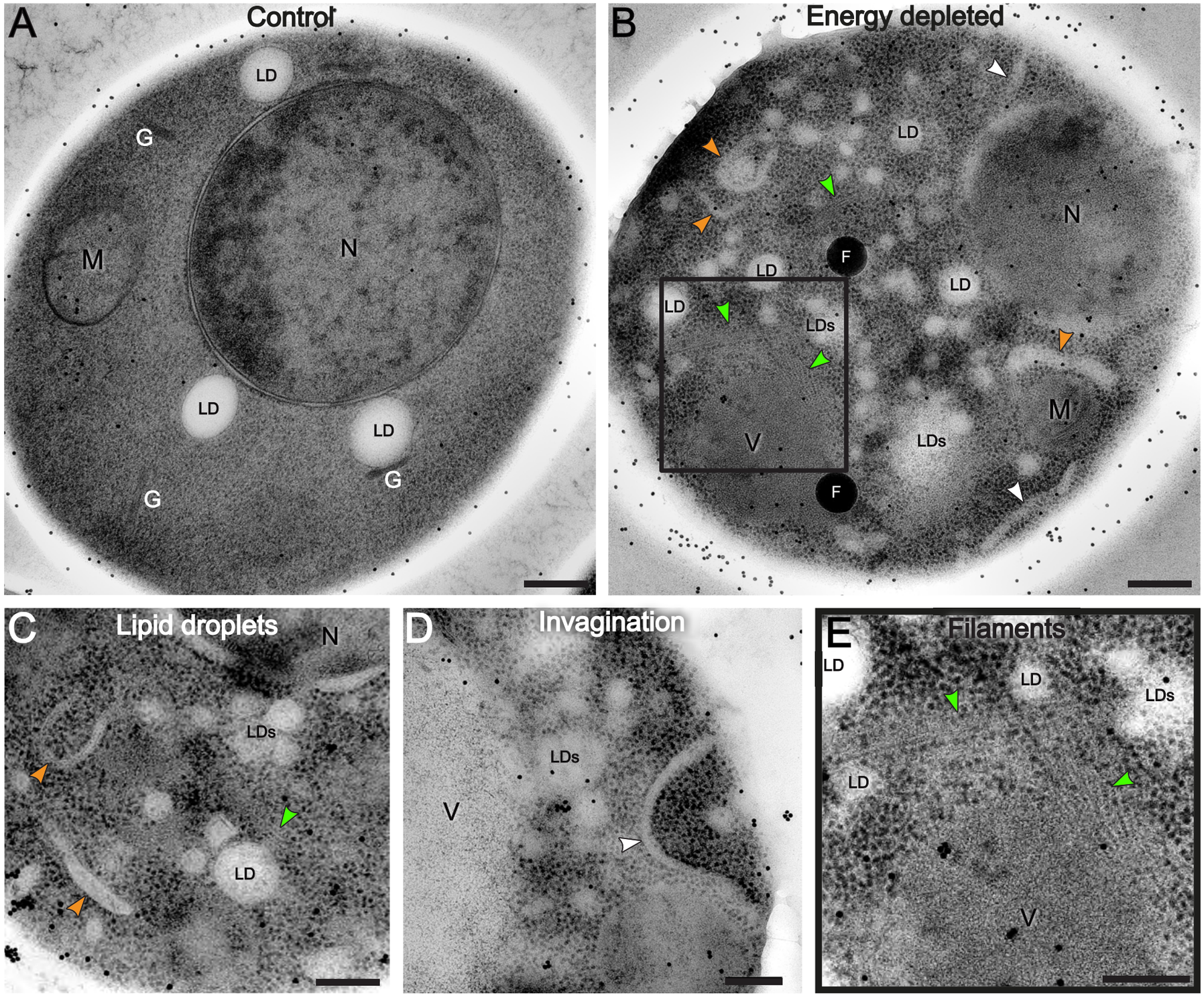

Figure 1. TEM images reveal cytoplasm reorganization in dormant yeast cells. Comparison between log-phase growing (A) and dormant (energy-depleted) (B,C,D,E) yeast cells show that many structures in the cytoplasm undergo a drastic reorganization. (E) Magnified inset from (B). Ribosomes appear densely packed in dormant cells (B,C,D,E), compared to control cells (A). Dormant cells contain numerous fragmented lipid droplets (LD, smaller droplets are not labeled) and irregularly shaped membranous structures (orange arrows) (B,C), elongated invagination of the cell membrane (white arrows) (B,D), and filamentous structures are visible in several parts of the cell (green arrow) (B,C,E). Scale bars: A,B = 300 nm; C,E = 200 nm. N = nucleus, M = mitochondria, G = Golgi, LD(s) = lipid droplet(s), V = vacuole, F = fiducial beads.

Fig. 2

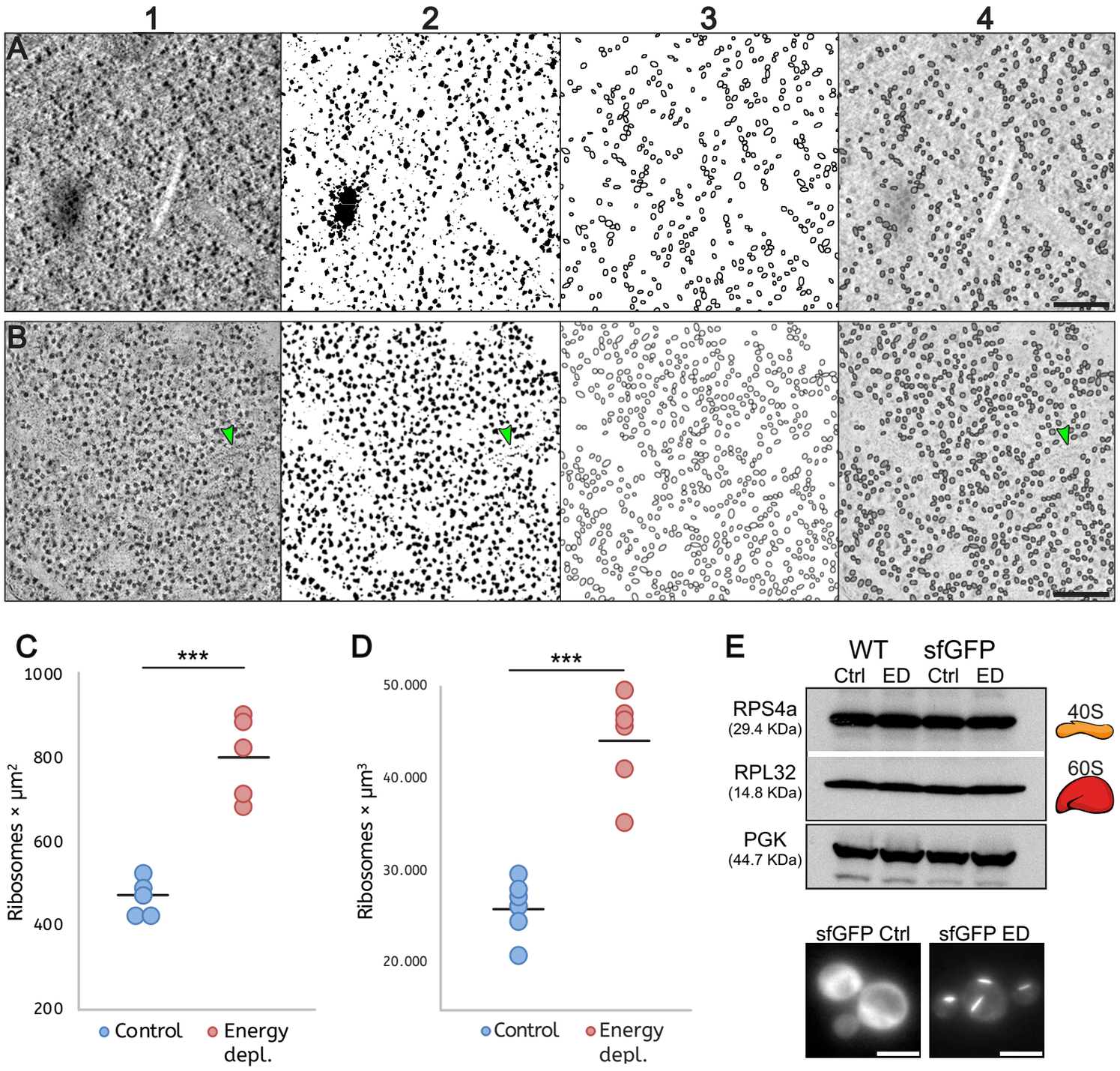

Figure 2. Quantification of ribosome density demonstrates macromolecular crowding in energy-depleted cells. (A-B) Automated pipeline for the quantification of ribosomes in tomograms, involving sequential (1) filtering, (2) binarization, (3) segmentation, and (4) particle detection on single slices through a tomogram from a cell in (A) control conditions and (B) following energy depletion. The green arrows in (B2 and B3) indicate a filament. (C-D) The ribosome number is increased almost two-fold in the energy-depleted cells. (C) Ribosome density in tomographic slices. Five tomograms were analyzed per condition. ***P-value = 0.0001. (D) Ribosomes density by manual counting in tomographic volumes. Six tomograms were analyzed per condition. ***P-value = 0.0001. (E) Western blot showing equal amounts of RPS4a (40S) and RPL32 (60S) ribosomal subunits in log-phase growing (Ctrl) and energy-depleted (ED) cells, in both wild-type and GFP-tagged eIF2B strains. 3-phosphoglycerate kinase (PGK) was used as a loading control. Cells expressing GFP-tagged eIF2B were imaged before Western blot analysis to validate the log-phase growth (diffuse GFP signal- GFP Ctrl) and the dormant, energy-depletion conditions (condensed GFP signal - GFP ED). Scale bars: A-B = 200 nm; E = 5 µm.

Fig. 3

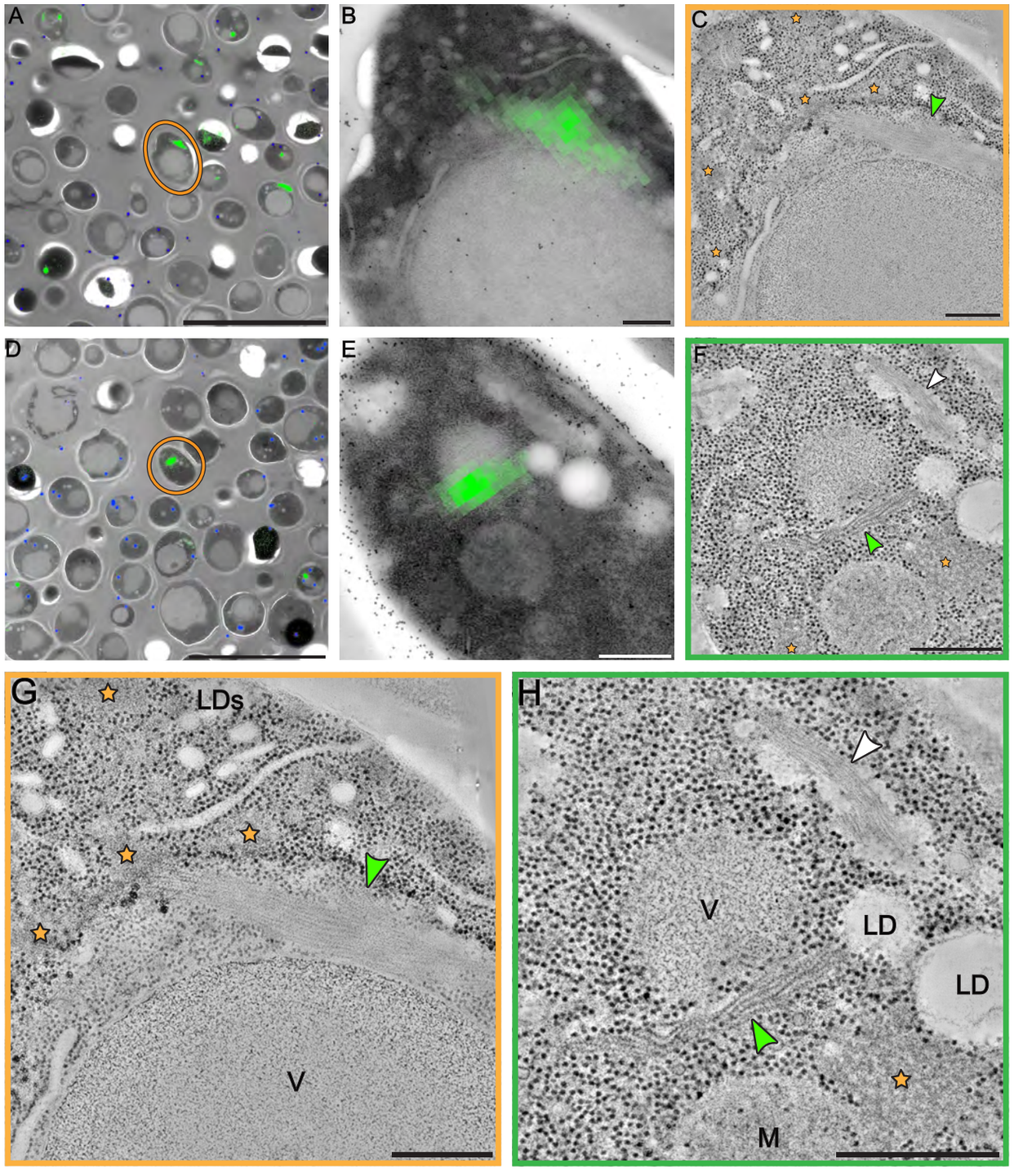

Figure 3. Correlative fluorescence and electron microscopy analysis reveals organization of GFP-tagged eIF2B into bundles of parallel filaments. (A, D) The fluorescent signal of GFP-eIF2B is overlaid on low-magnification TEM images of energy-depleted yeast cells previously embedded in Lowicryl HM-20 and then sectioned. The orange circles highlight cells that were selected for further tomographic analysis. (B, E) Close up of the cells highlighted in A and D, respectively. (C,F,G,H) Slices through tomographic reconstructions of the same cells as in B and E. (G,H) Magnified views of the tomographic slices shown in C and F, respectively. Bundles of filamentous structures (green arrows) corresponding to the fluorescence signal. eIF2B organizes in ordered, non-membrane-bound arrays of filaments. Energy-depleted cells also contain other non-membrane-bound compartments that do not include ribosomes. Some have an amorphous appearance (orange stars), whereas others comprise filamentous structures (H) (white arrow). These filaments, which do not display a fluorescent signal, have a different morphology to the eIF2B filaments and their protein content is unknown. LD(s) = lipid droplet(s); M = mitochondrion; V = vacuole. Scale bars: A, D = 10 µm; B-C, G = 200 nm; E-F, H = 500 nm.

Fig. 4

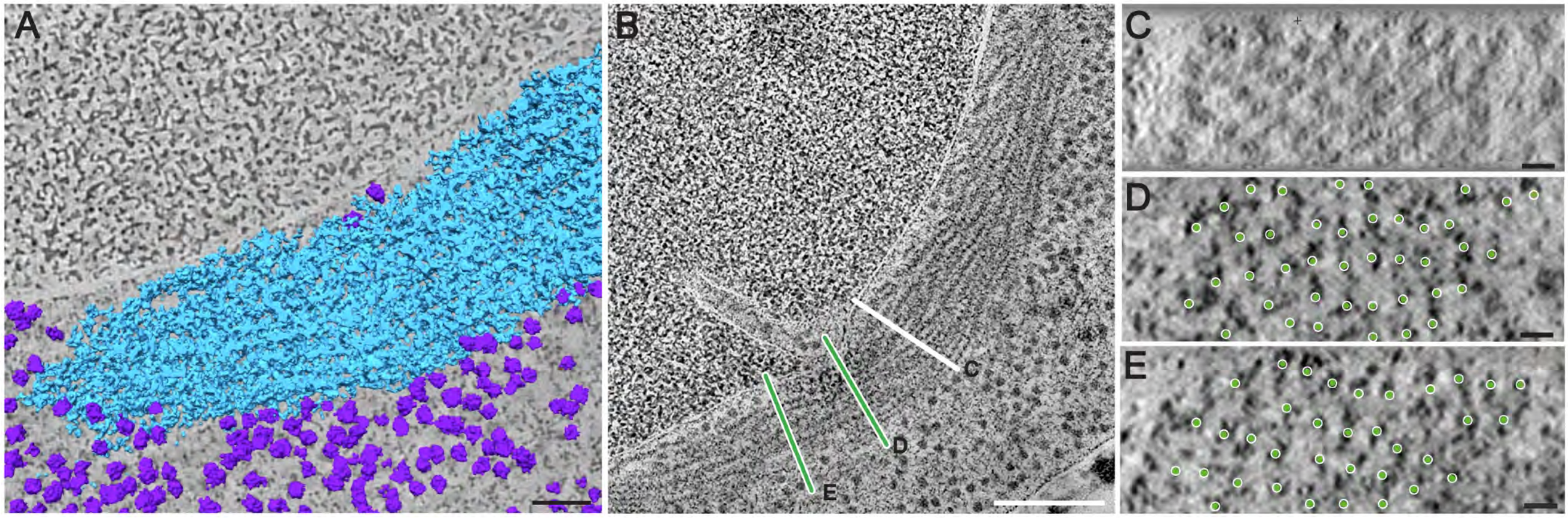

Figure 4. Segmentation and cross-sectional views of a eIF2B bundle showing the ordered arrangement of eIF2B filaments. (A) Automated segmentation of ribosomes (purple) and eIF2B filaments (cyan) in the tomographic reconstruction of a cell overexpressing GFP-tagged eIF2B, (B) Tomographic slice through a larger field of view of the same tomogram. eIF2B filaments are packed with a roughly parallel arrangement in a bundle. White and green lines indicate cutting planes through the bundle corresponding to the cross-sectional view in C, D, and E. (C, D, E) Cross-sectional views of the filaments in the bundle in B. eIF2B filaments follow a regular pattern with a center-to-center inter-filament spacing of approximately 20 nm. The green dots in D and E show the coordinates of each filament that was automatically detected and traced with the Amira® software. Scale bars: A = 50 nm; B = 200 nm; C, D, E = 20 nm.

Fig. 5

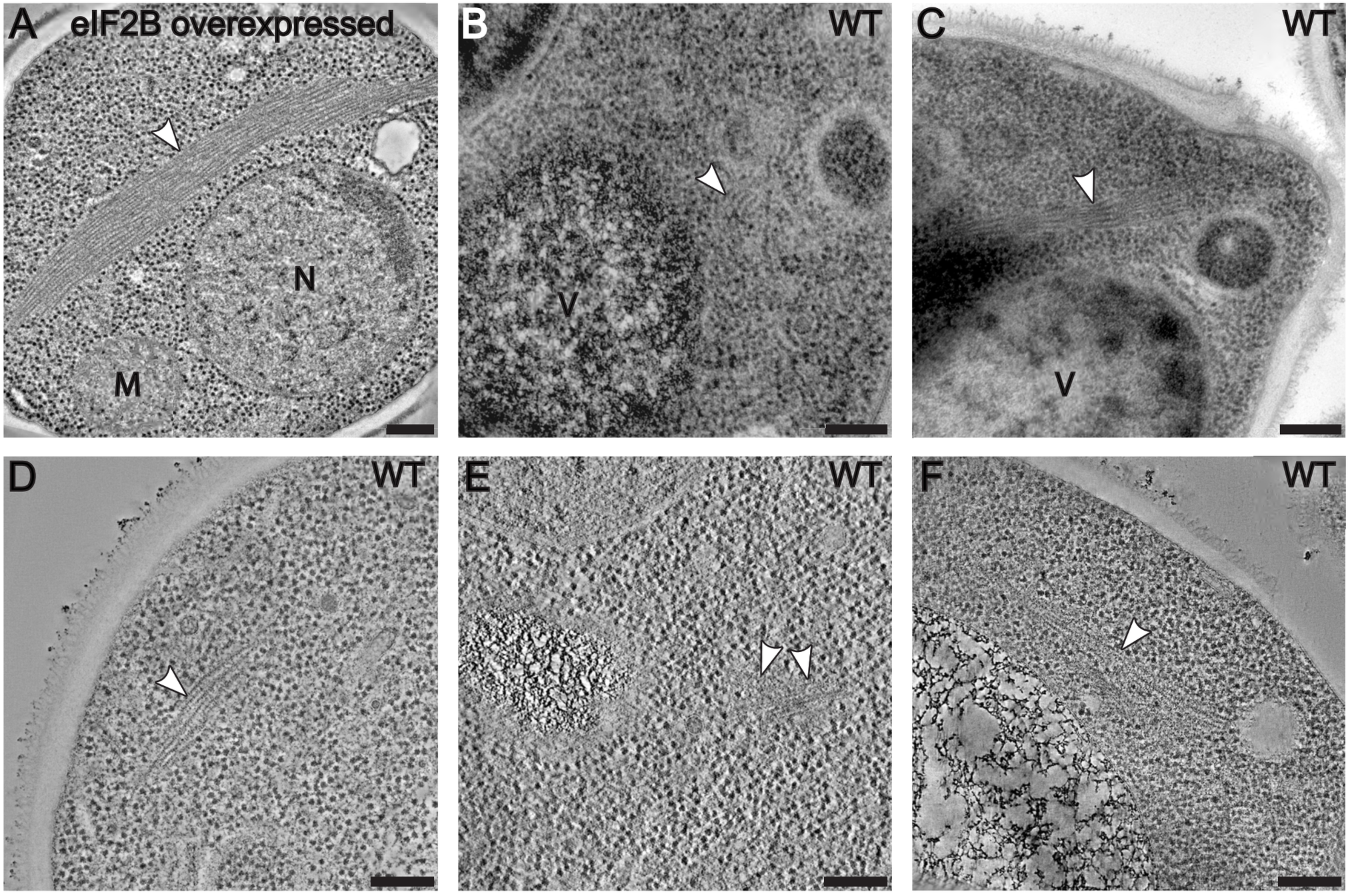

Figure 5. Untagged eIF2B forms filaments and bundles in energy-depleted yeast cells. Averages of 20 tomographic slices of yeast cells showing (A) overexpressed eIF2B forming large bundles of filament in the cytoplasm, and (B-F) endogenously expressed eIF2B forming smaller bundles of filaments in the cytoplasm of wild type yeast cells. Scale bars = 200 nm.

Fig. 6

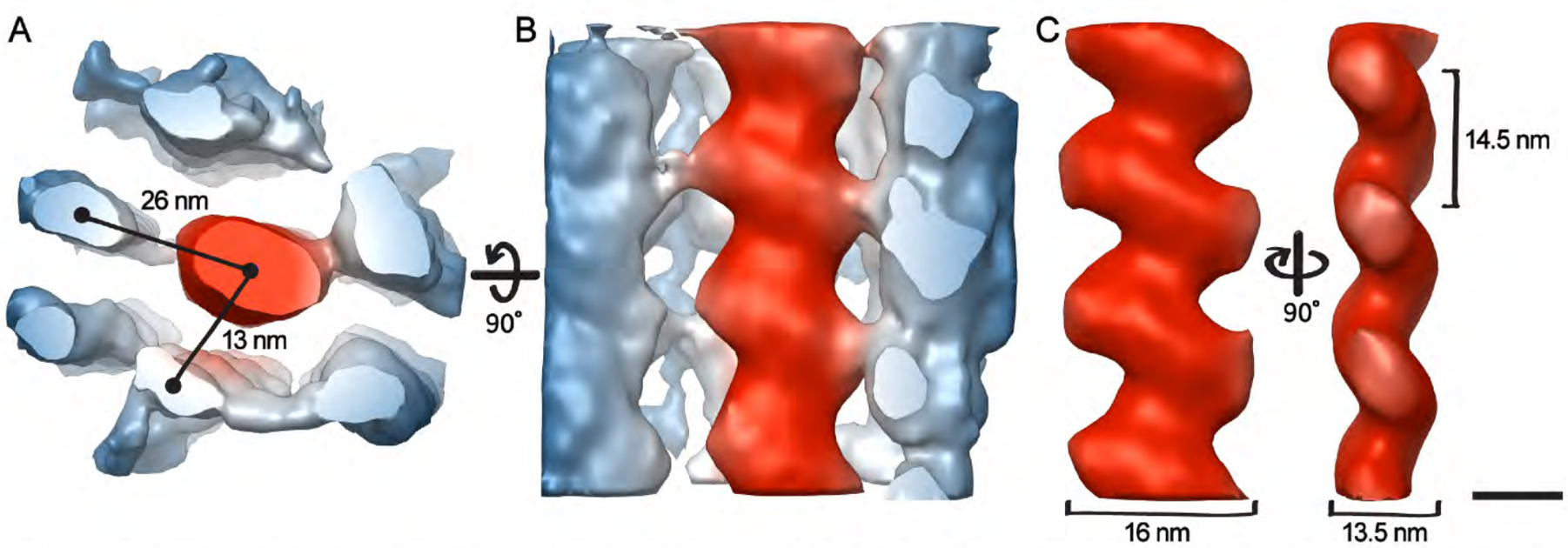

Figure 6. 3D organization of parallel filaments in the eIF2B bundle reveals lateral connections. (A-C) Subtomogram averaging of three repeating units along an eIF2B filament. (A-B) Neighboring filaments (in blue) are still visible in the average, which is indicative of their roughly consistent position around a central filament (in red). The center-to-center distance between the central filament and the surrounding ones is ~26 nm for filaments in the same row and ~13 nm for filaments in parallel rows. (B) The longitudinal view of the central filaments has a zigzag shaped structure. Lateral connections are visible between the central filament and the surrounding ones. (C) The filament shows a 14.5 nm repeat, a long diameter of 16 nm and a short diameter of 13.5 nm. (D) Average of 10 tomographic slices showing the eIF2B bundle used for the 3D model reconstruction of the filaments and the periodicity at which particles have been picked (white lines). Scale bars: A,B,C = 10 nm; D = 200 nm.

Fig. 7

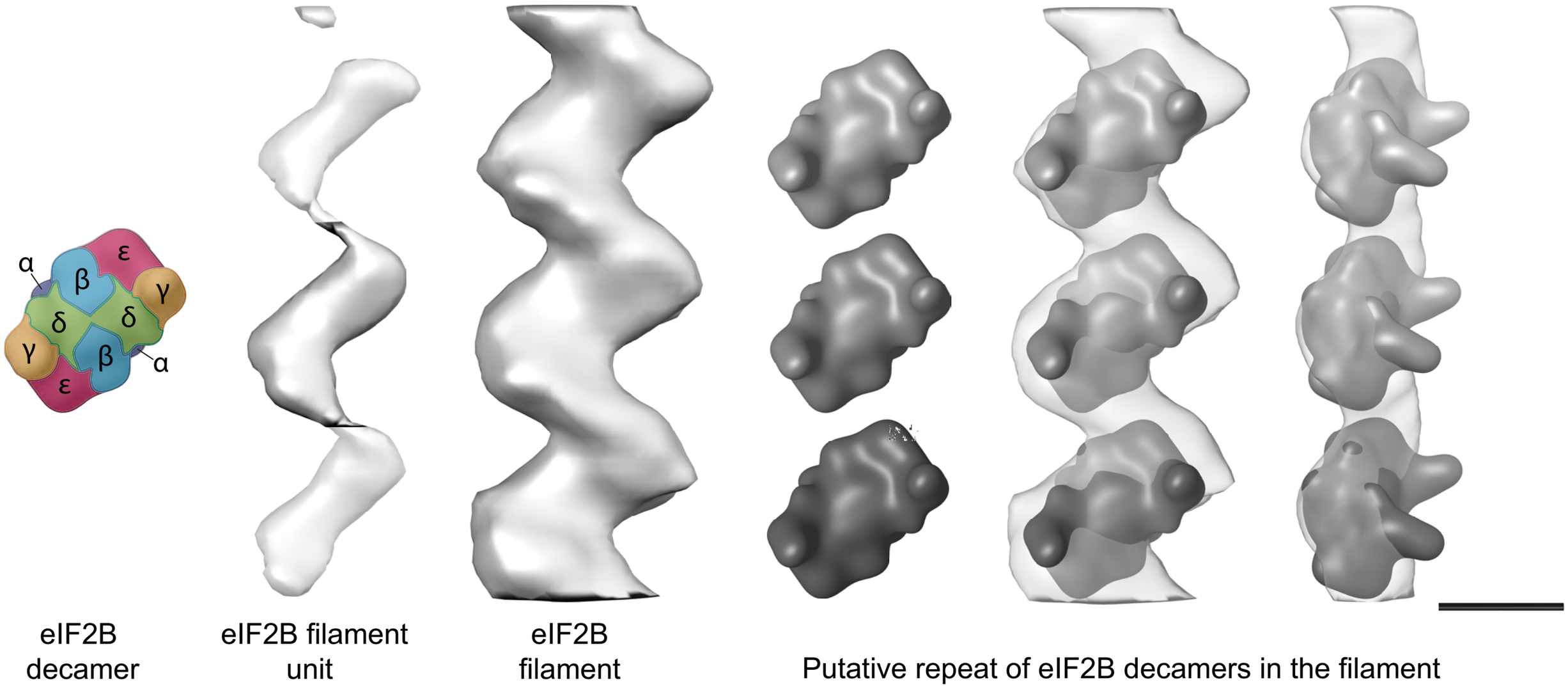

Figure 7. Proposed organization of eIF2B decamers in the filament. The repeating units in eIF2B filaments have a size and overall shape similar to the heavily filtered density map of the eIF2B decamer; blue = Gcn3 (α) subunit, cyan = Gcd7 (β) subunit, orange = Gcd1 (γ) subunit, green = Gcd2 (δ) subunit, magenta = Gcd6 (ε) subunit. The rough alignment of three density maps with the filament 3D model suggests a possible stacking of eIF2B decamers in the polymerized form. Scale bar= 10 nm

Fig.8

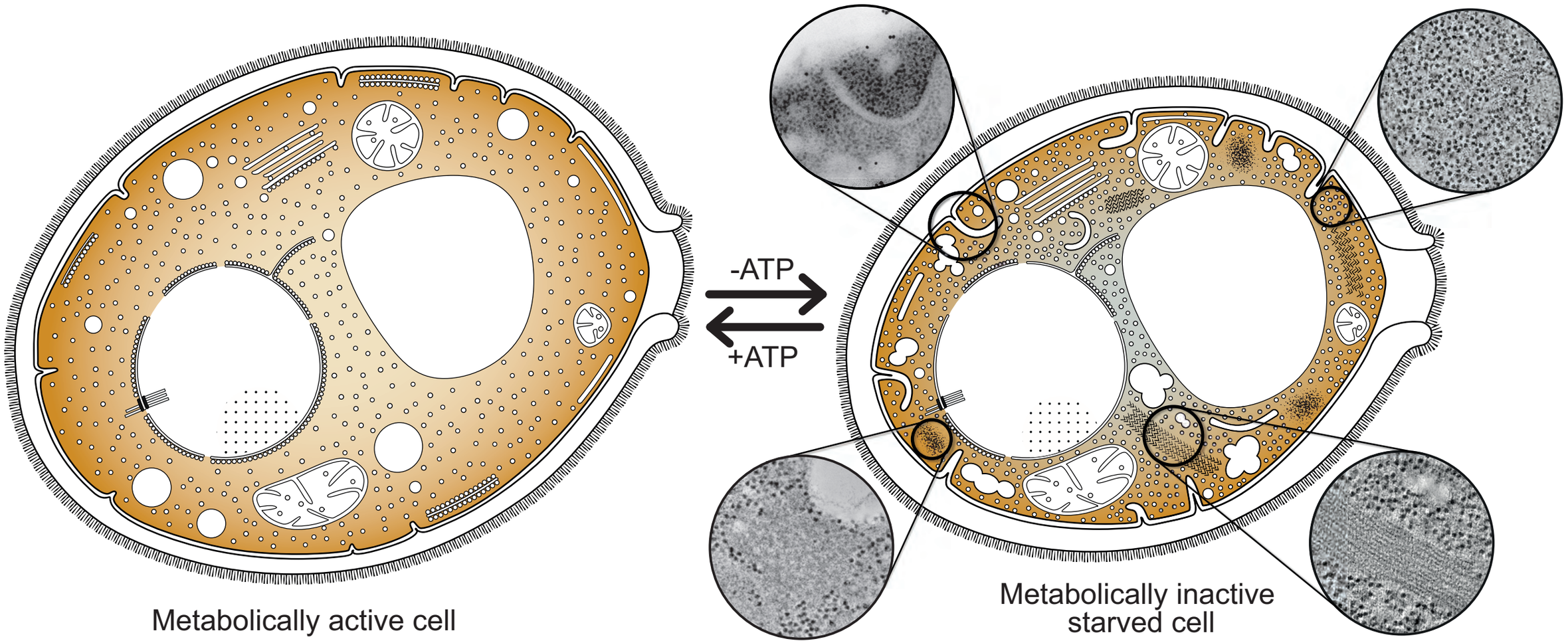

Figure 8. Cytoplasm solidification functions as a protective state of energy-depleted cells. Ultrastructural analysis shows that energy depletion induces a striking reorganization of cytoplasmic structures in yeast cells. ATP-depleted cells undergo cell volume reduction, with consequent formation of plasma membrane invaginations (1) and a pronounced increase in macromolecular crowding (2). Numerous non-membrane bound compartments with amorphous (3) or highly ordered morphologies, such as the ones formed by eIF2B (4), appear in the cytoplasm. These are indicative of phase separation processes that enable storage of macromolecules in depots, as well as concentrated biochemistry. Energy-depleted cells are also characterized the fragmentation of lipid droplets, suggesting a switch to beta-oxidative metabolism. All these cellular rearrangements result in a “solidification” of the cytoplasm that protects essential molecular components, which are thus readily available as favourable environmental conditions are restored.

Figure S1

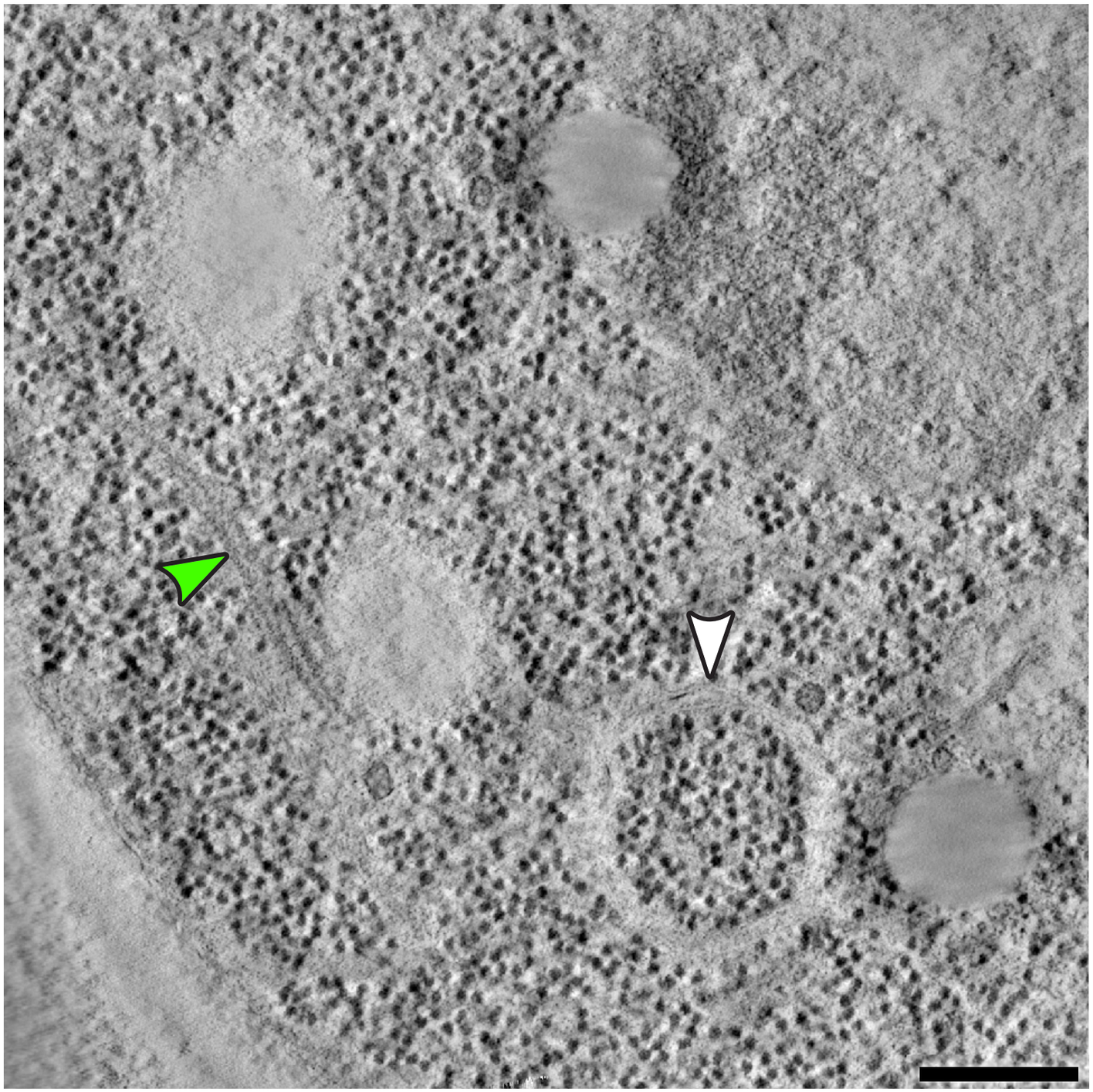

Figure S1. Vesicle containing ribosomes in a stressed yeast cell. A double membrane vesicle, highlighted with a white arrow, contains tightly packed ribosomes visible in the lumen. Due to its reduced size (~300 nm), it might be identified as an early autophagosomal vesicle, probably in the process of bringing its content to the vacuole for degradation. The green arrow points to a filament in the cytoplasm. Scale bar = 200 nm.

Video S1

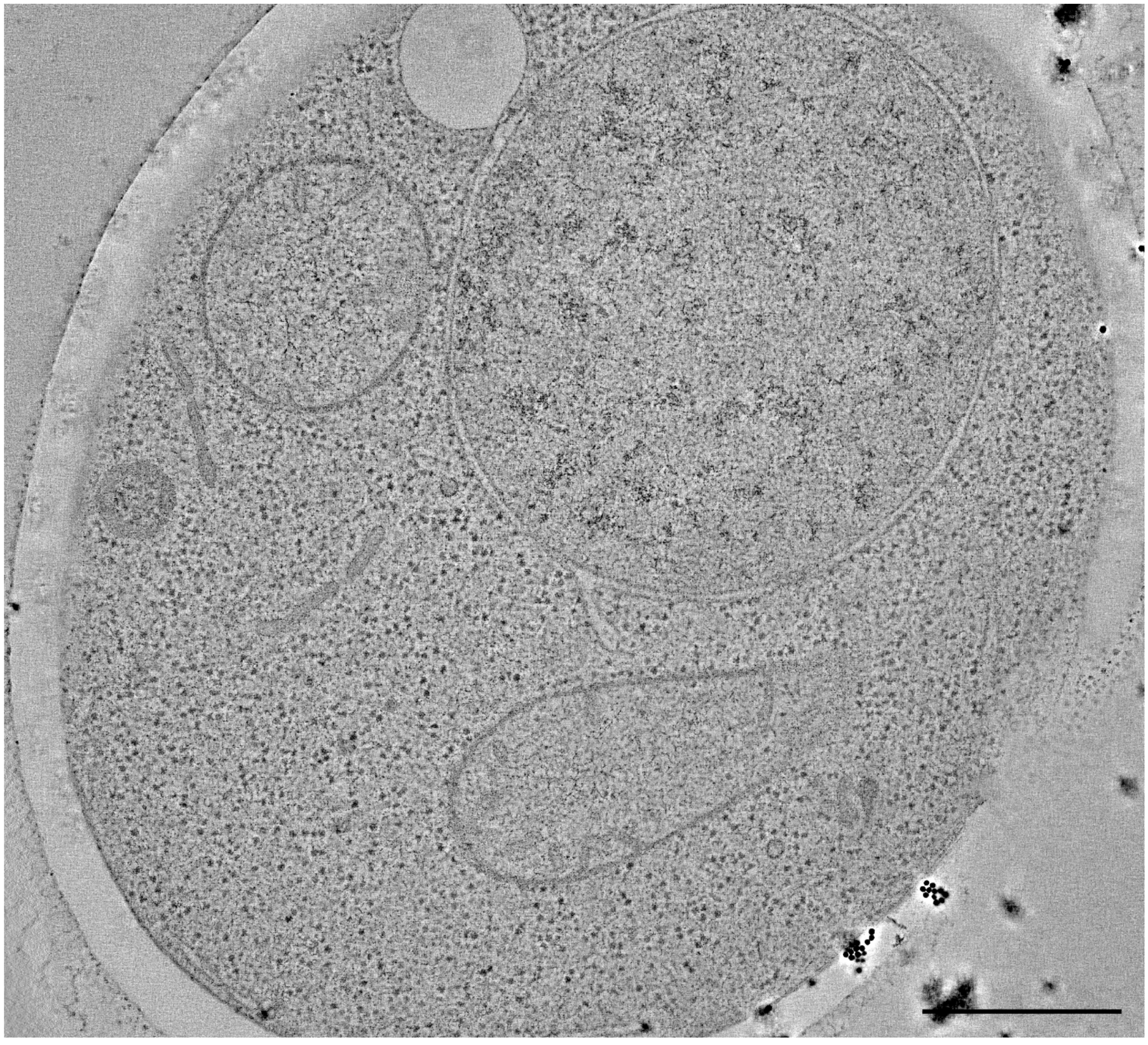

Video S1. 3D tomographic reconstruction of a non-stressed yeast cell. Scale bar= 500 nm

Video S2

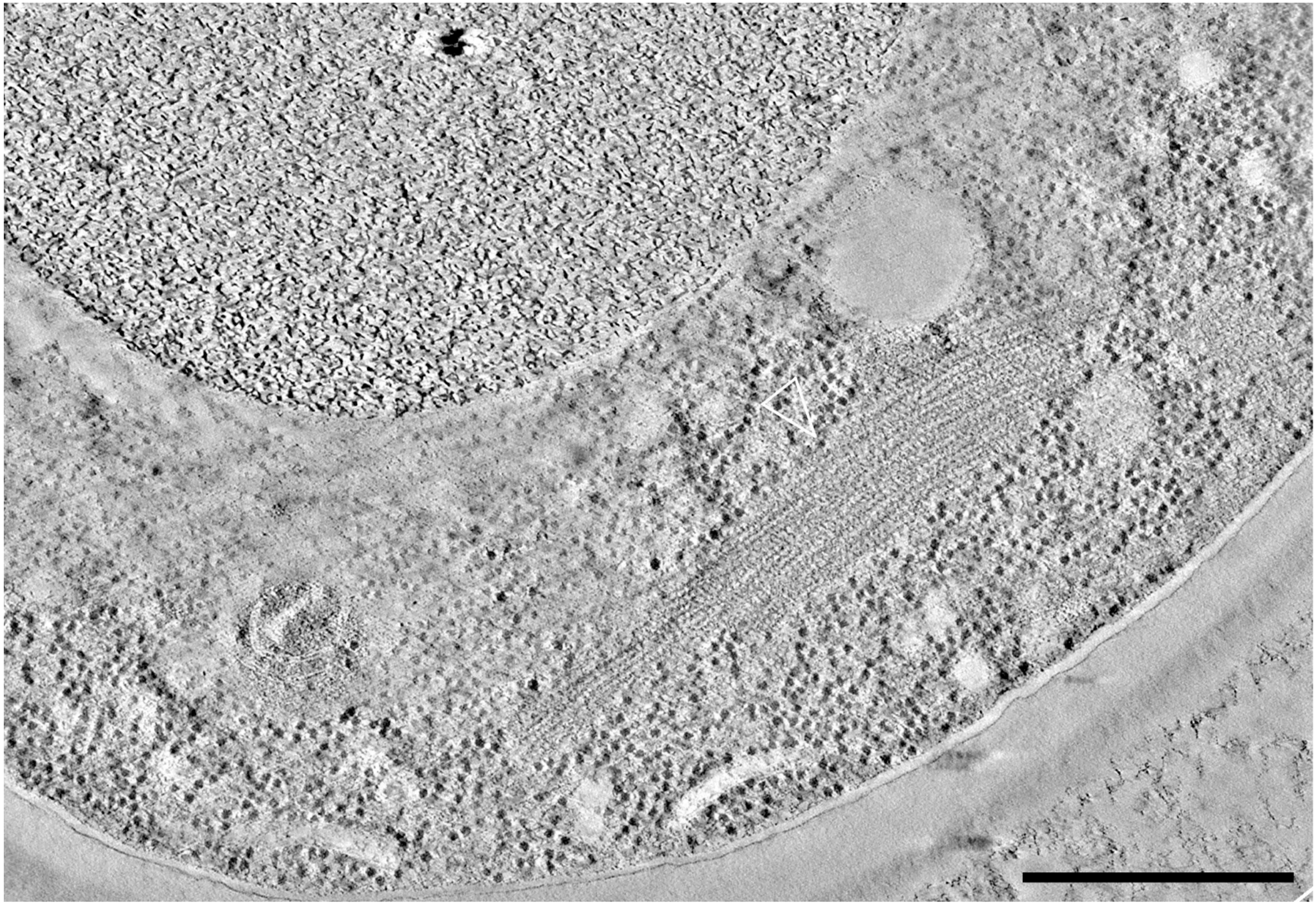

Video S2. 3D tomographic reconstruction of a 15 minutes energy-depleted yeast cell. eIF2B is unlabelled and over-expressed. Scale bar= 500nm

Video S3

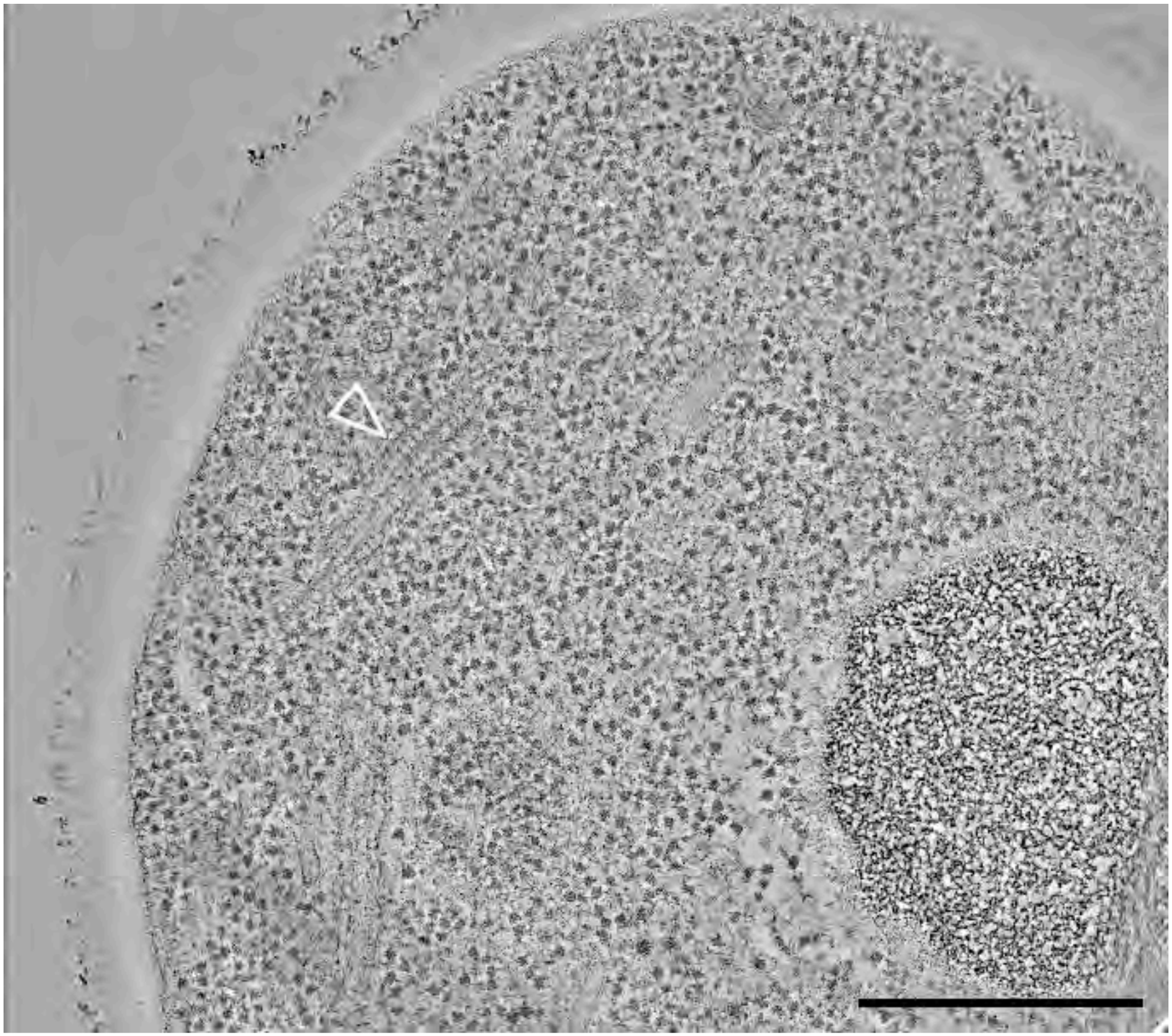

Video S3. 3D tomographic reconstruction of an energy-depleted yeast cell. eIF2B is unlabelled and endogenously expressed. Scale bar= 500nm

Fig.S2

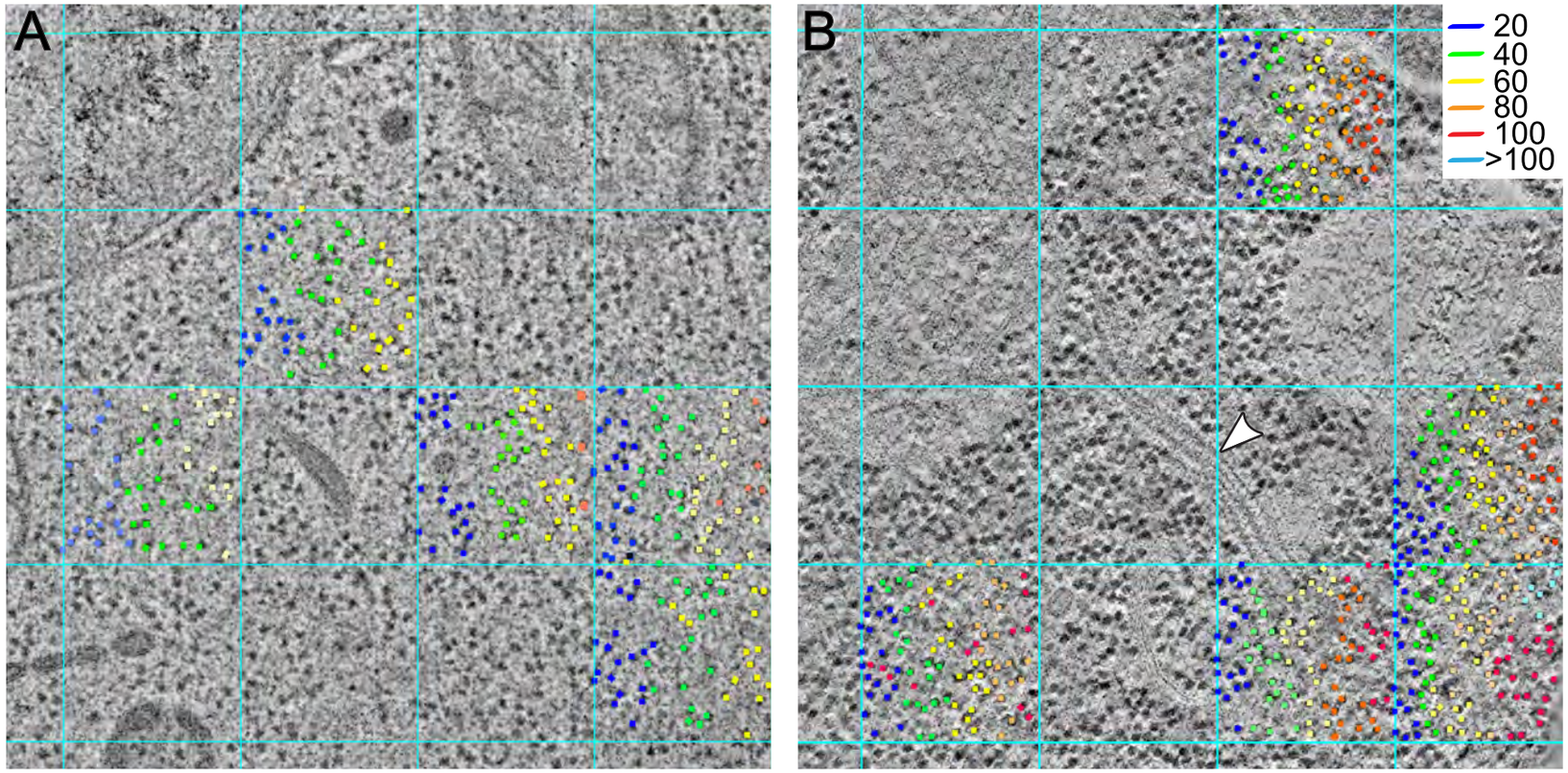

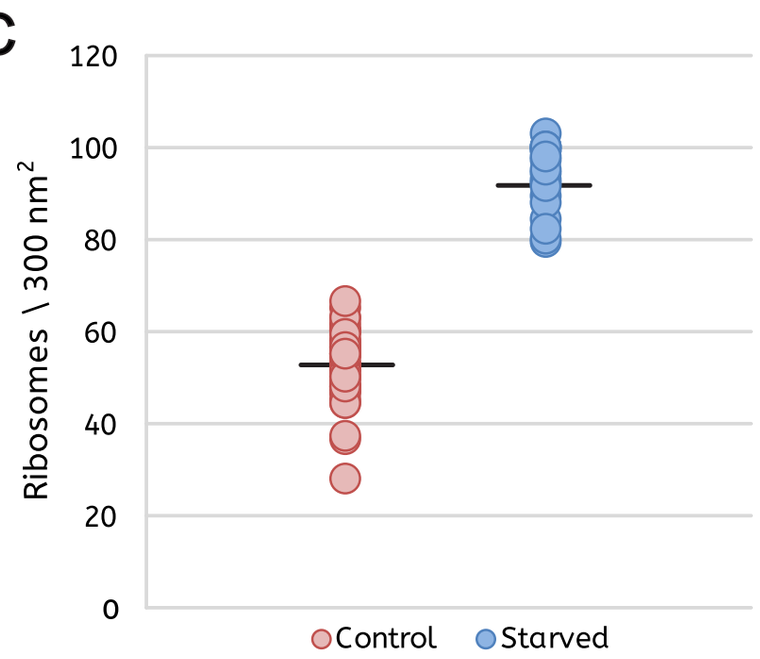

Figure S2. Manual method for ribosome counting. A 300 × 300 nm grid is superimposed on the central slice of a tomogram. Ribosomes in 5 randomly chosen squares are counted. Only ribosomes in the upper and left edge of each chosen square are included in the count. (A) Yeast control cells have usually 50-70 ribosomes per 300 nm^2 area. (B) Energy depleted yeast cells have usually 100 or more ribosomes per 300 nm^2 area. White arrow highlights a filament in the stressed cell. (C) The result of the manual ribosome counting is shown in the plot. Five tomograms are analyzed for each condition. The almost-two-fold increase (42%) in ribosome density in the stressed yeast cells is confirmed.

Fig.S3

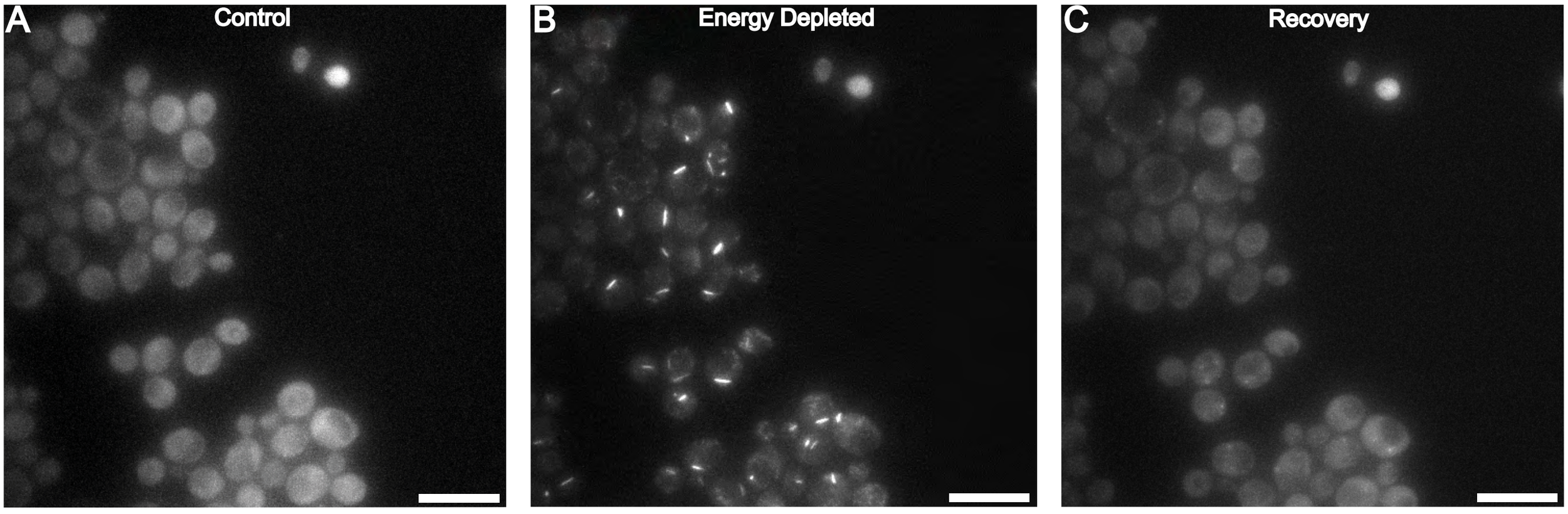

Figure S3. eIF2B enzymes change their cytoplasmic distribution between log-phase growing and energy-depleted yeast cells. (A) According to the fluorescent signal, the GFP-labeled eIF2B complexes have a diffuse distribution throughout the cytoplasm in log-phase growing and dividing cells. (B) The fluorescence signal of GFP-tagged eIF2B condenses into foci-like or elongated structures in stressed cells that have been energy-depleted for 15 minutes. (C) The fluorescence signal rapidly recovers a diffuse distribution as cells reenter the cell cycle upon energy replenishment. Scale bars =10 μm.

Video S4

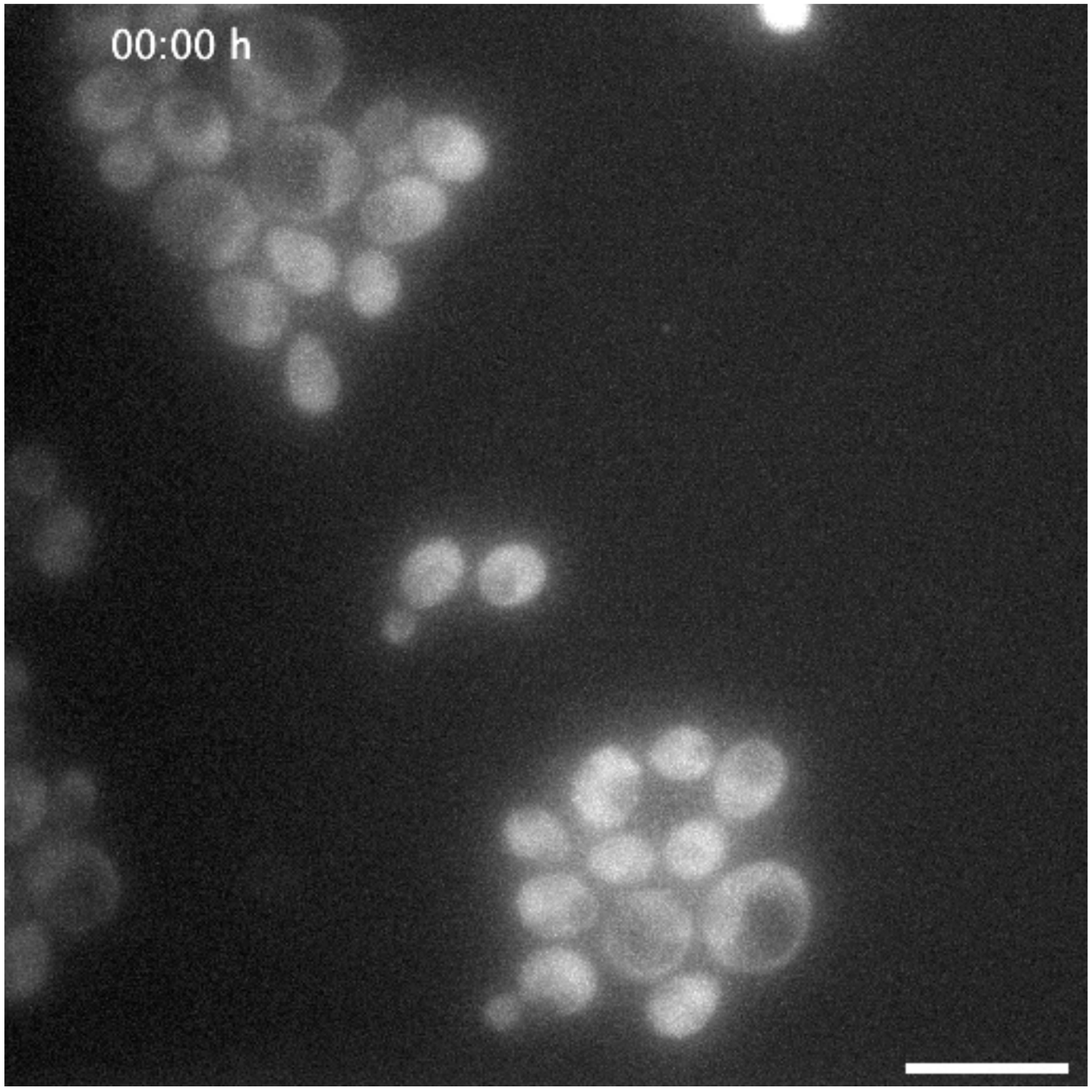

Video S4. The fluorescent signal of eIF2B is distributed differently between stressed yeast cells and log-phase growing cells. According to the fluorescent signal, the GFP-labeled Gcn3 (α) subunit of eIF2B present a diffuse distribution throughout the cytoplasm in log-phase growing and dividing cells. On the contrary, the fluorescence is concentrated into condensed foci-like or elongated structures in stressed cells that have been energy depleted for 15 minutes at pH 5.5. Scale bar= 10 μm

Fig.S4

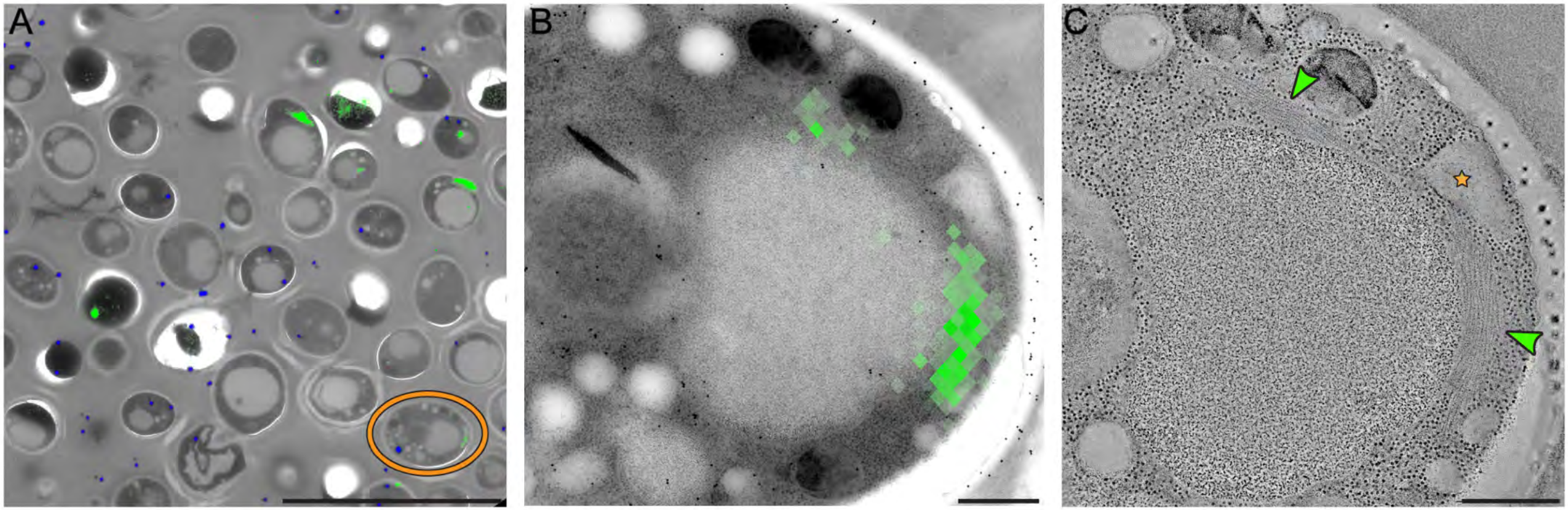

Figure S4. Correlative fluorescence and electron microscopy analysis reveals organization of GFP-tagged eIF2B into bundles of parallel filaments. (A) The fluorescent signal of GFP-eIF2B is overlaid on low-magnification TEM image of energy-depleted yeast cells previously embedded in Lowicryl HM-20 and then sectioned. (B) Close up of the cell highlighted in A. (C) Magnified views of the tomographic slices shown in C. Two bundles of filamentous structures (green arrows) corresponds to the fluorescence signal. Another non-membrane-bound compartment with amorphous appearance is labelled with an orange star. Scalebars: A=10 µm, B, C=500 nm.

Video S5

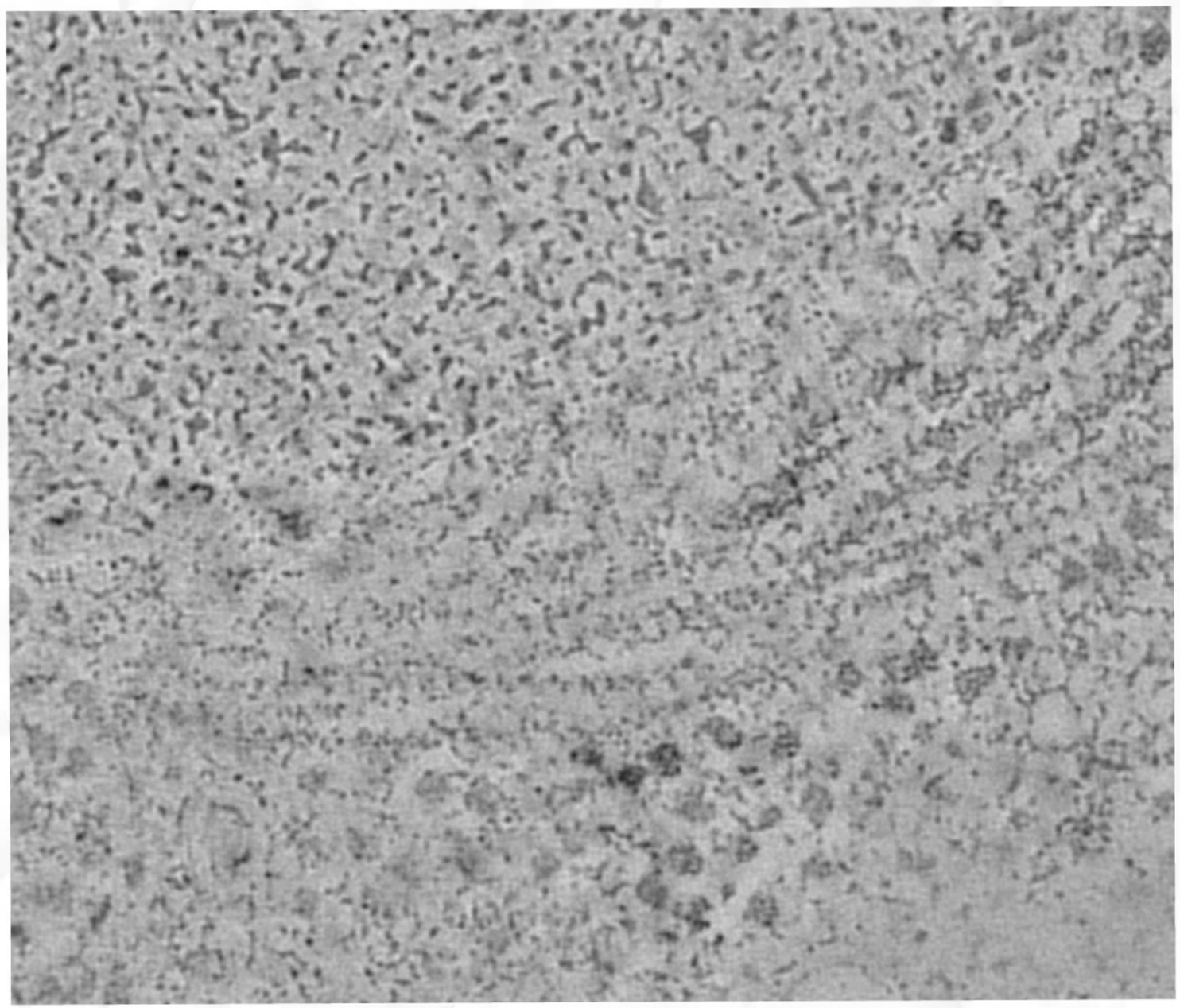

Video S5. Segmentation of a bundle of eIF2B filaments in a reconstructed tomogram using Super Region Volume Segmentation software [Luengo et al., 2017]. Automated segmentation of ribosomes (purple) and eIF2B filaments (cyan) in the tomographic reconstruction of a cell overexpressing GFP-tagged eIF2B.

Figure S5

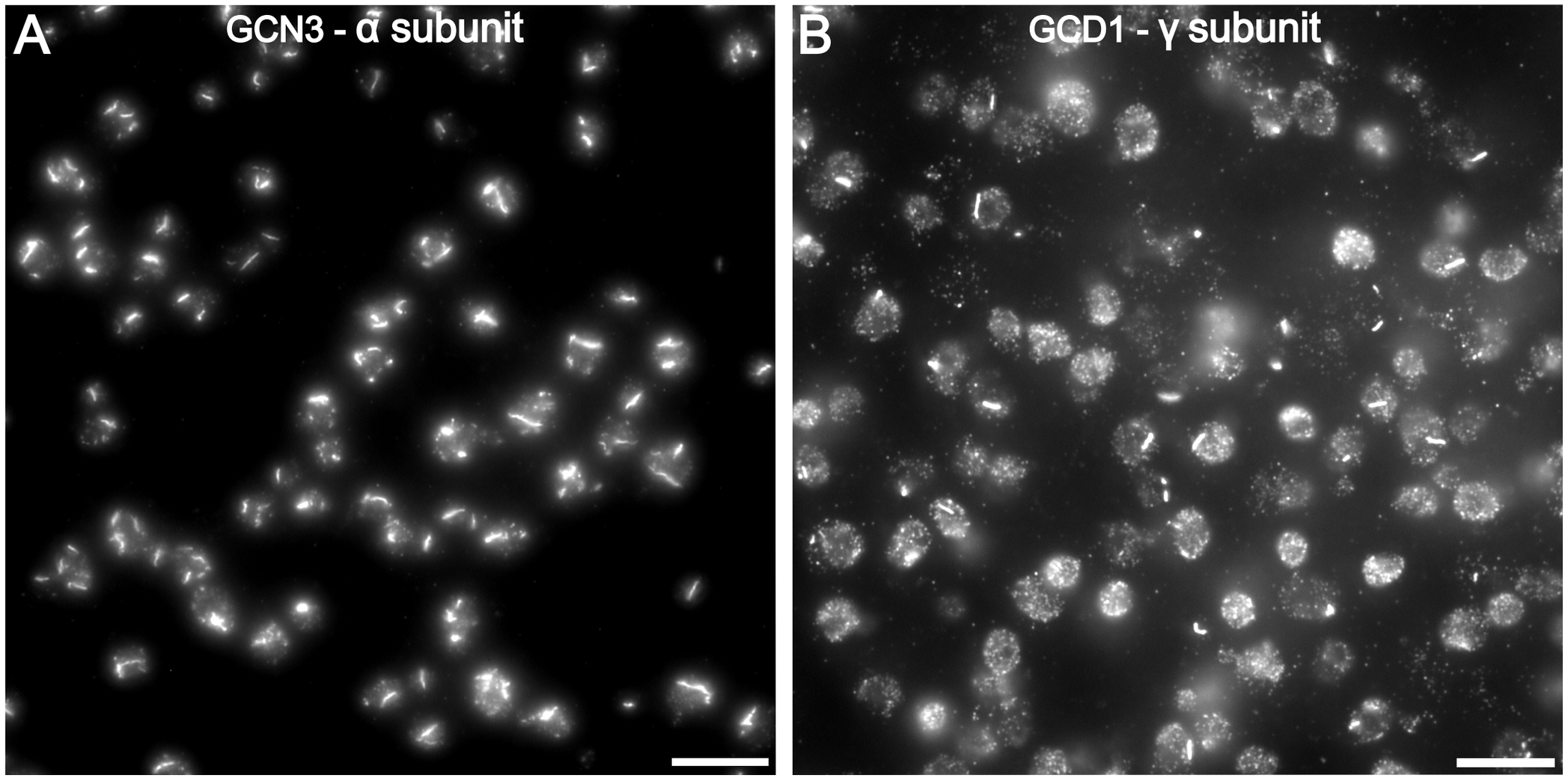

Figure S5. Immunofluorescence labeling of two HA-tagged eIF2B subunits show filament bundles in energy-depleted yeast cells. (A) Immunolabeling of the HA-tagged GCN3 (α) and (B) GCD1 (γ) subunits of eIF2B show that the formation of filament bundles in energy-depleted cells occurs in the absence of the GFP-tag. This demonstrates that separation of eIF2B in non-membrane bound compartments is not induced or enhanced by the GFP-tag. Scale bars = 10 μm.